
Article:
Susmel, L. orcid.org/0000-0001-7753-9176 (2022) Notches, nominal stresses, fatigue strength reduction factors and constant/variable amplitude multiaxial fatigue loading. International Journal of Fatigue, 162. 106941. ISSN 0142-1123

https://doi.org/10.1016/j.ijfatigue.2022.106941

International Journal of Fatigue xxx (xxxx) xxx

Contents lists available at ScienceDirect

International Journal of Fatigue

journal homepage: www.elsevier.com/locate/ijfatigue

Notches, nominal stresses, fatigue strength reduction factors and constant/variable amplitude multiaxial fatigue loading

Luca Susmel

Department of Civil and Structural Engineering, The University of Sheffield, Mapping Street, Sheffield S1 3JD, UK

ARTICLE INFO

Keywords:
Nominal stress
Fatigue strength reduction factor
Critical plane
Multiaxial loading
Variable amplitude

ABSTRACT

This paper deals with the reformulation of the Modified Wöhler Curve Method to make it suitable for being used along with nominal stresses to design notched components against constant/variable amplitude multiaxial fatigue loading. The accuracy of this design methodology is checked against a large number of experimental results taken from the literature. The outcomes of the performed validation exercise strongly support the idea that the proposed approach can safely be used to perform the multiaxial fatigue assessment of notched structural components. This holds true also when the necessary fatigue strength reduction factors are estimated via standard, classic formulas.

1. Introduction

The constituting structural elements of mechanical assemblies and structures have complex geometries that result in localised stress/strain concentration phenomena. These notched structural components are often subjected to time-variable loading that can lead to the initiation and propagation of fatigue cracks. Under very specific circumstances, the in-service load paths comprise constant amplitude (CA) fatigue cycles. However, in most situations of practical interest structural components are subjected to variable amplitude (VA) load spectra. On the top of that, the fatigue design problem is further complicated by the fact that, in general, real in-service load histories are multiaxial in nature.

As far as un-notched metallic materials subjected to CA multiaxial fatigue loading are concerned, examination of the state of the art shows that a good level of accuracy can be reached using a variety of design criteria [1]. However, despite such an encouraging degree of design reliability, it is evident that more work needs to be done in order to better incorporate the effect of the material microstructure into the fatigue design process [2]. In this context, the key issue is that materials with different levels of ductility show a different sensitivity to the degree of non-proportionality of the applied load history [3].

While an enormous amount of work has been done to investigate the multiaxial fatigue behaviour of plain metallic materials, so far the international scientific community has given way less attention to the multiaxial notch fatigue problem [4-7]. As far as geometrical stress/strain concentrators are concerned, the knowledge available in the technical literature suggests that the most effective design methodologies are those based on the combined use of local (linear-elastic or elasto-plastic) stress/strain fields and material length scale parameters [8-13]. In this setting it is important to point out that a number of systematic attempts have been made also to develop specific approaches suitable for designing notched metallic materials against VA multiaxial fatigue loading [14-17]. Clearly, the latter design problem is very relevant in situations of practical interest since, as a matter of fact, real structural components are not only notched, but also subjected to in-service VA multiaxial load histories.

While multiaxial fatigue is still a very popular research topic, the enormous amount of work briefly summarised above has already resulted over the years in a number of very detailed guidelines and recommendations (such as, for instance, Refs [18-21]) that allow multiaxial fatigue assessment of un-welded and welded components to be performed by reaching an adequate level of safety.

Turning back to the problem of designing notched structural components against multiaxial fatigue, while local stress/strain-based approaches are seen to return reliable, accurate estimates, their usage in situations of industrial interest is never straightforward. A major limitation is that the stress/strain fields in the vicinity of the geometrical features being designed must be determined in a very accurate way. In this context, certainly the finite element (FE) method is the most effective approach to be used to perform the stress/strain analysis in the presence of complex, three-dimensional geometrical features [22]. However, its industrial usage is somehow limited by the fact that the determination of the necessary local stress/strain fields can require very

Abbreviations: Ax, axial loading; CA, constant amplitude; IPh, in-phase loading; MWCM, modified Wöhler curve method; OoPh, out-of-phase loading; To, torsion; τ-MVM, shear stress-maximum variance method; VA, variable amplitude.

https://doi.org/10.1016/j.ijfatigue.2022.106941
Received 10 January 2022; Received in revised form 17 April 2022; Accepted 18 April 2022
Available online 21 April 2022

Nomenclature

a_H	material constants in Heywood's relationships
a_P, a_{Pt}	material lengths in Peterson's relationships
d_n, d_g	diameters of the notched specimens
k	negative inverse slope of the uniaxial Wöhler curve
kτ	negative inverse slope of the modified Wöhler curve
k_0	negative inverse slope of the torsional Wöhler curve
m	mean stress sensitivity index
m_τ	negative inverse slope of the modified Wöhler curve for $N_f > N_{kp}$
n_i	number of cycles at a shear stress level equal to $\tau a_{,i}$
q	notch sensitivity factor
r_n	notch root radius
D_{tot}	total value of the damage sum
D_{cr}	critical value of damage sum D_{tot}
F	ratio between the frequencies of the applied axial and torsional nominal loading
F_a	amplitude of the axial force
K_f	fatigue strength reduction factor under either axial loading or bending
$K_{f,est}$	estimated value of K_f
$K_{f,exp}$	experimental value of K_f
K_{ft}	fatigue strength reduction factor under torsional loading
$K_{ft,est}$	estimated value of K_{ft}
$K_{ft,exp}$	experimental value of K_{ft}
K_t	stress concentration factor referred to the net area under either axial loading or bending
K_{tt}	stress concentration factor referred to the net area under torsional loading
T_a	torque amplitude
N_f	number of cycles to failure
$N_{f,e}$	estimated number of cycles to failure
$N_{f,i}$	number of cycles to failure at a shear stress level equal to $\tau a_{,i}$
N_{kp}	number of cycles to failure defining the position of the knee point
N_A	reference number of cycles to failure in the high-cycle fatigue regime
N_S	reference number of cycles to failure in the low-cycle fatigue regime
P_S	probability of survival
R	load ratio
T	observation period (time interval) of the load history
T_σ, T_τ	scatter ratio of endurance limit for 90% and 10% probabilities of survival
α	notch opening angle
$\sigma_{net,a}$	amplitude of the nominal normal stress referred to the net area
σ_0	uniaxial fatigue limit
σ_{0n}	notch uniaxial fatigue limit referred to the net area
σ_A	uniaxial endurance limit extrapolated at N_A cycles to failure
σ_{An}	notch nominal net uniaxial endurance limit extrapolated at N_A cycles to failure
$\sigma_n(t)$	instantaneous values of the stress perpendicular to the critical plane
$\sigma_{n,a}$	amplitude of the stress perpendicular to the critical plane
$\sigma_{n,m}$	mean stress perpendicular to the critical plane
$\sigma_{n,min}$	minimum value of normal stress $\sigma_n(t)$
$\sigma_{n,man}$	maximum value of normal stress $\sigma_n(t)$
σ_S, τ_S	reference stress in the low-cycle fatigue regime at N_S cycles to failure
σ_{UTS}	ultimate tensile strength
σ_Y	yield stress
ρ_{eff}	effective value of the critical plane stress ratio
ρ_{lim}	limit value of ρ_{eff}
$\tau(t)$	instantaneous value of the shear stress relative to the critical plane
τ_0	torsional fatigue limit
τ_{0n}	notch torsional fatigue limit referred to the net area
τ_a	shear stress amplitude relative to the critical plane
τ_m	mean value of the shear stress relative to the critical plane
$\tau_{a,i}$	amplitude of the i-th shear stress cycle
τ_A	torsional endurance limit extrapolated at N_A cycles to failure
τ_{An}	notch nominal net torsional endurance limit extrapolated at N_A cycles to failure
$\tau_{A,Ref}$	amplitude of the reference shear stress at N_A cycles to failure
$\tau_{MV}(t)$	instantaneous values of the shear stress resolved along the direction of maximum variance of the resolved shear stress
$\tau_{net,a}$	amplitude of the nominal shear stress referred to the net area
$\tau_{MV,min}$	minimum value of resolved shear stress $\tau_{MV}(t)$
$\tau_{MV,max}$	maximum value of resolved shear stress $\tau_{MV}(t)$

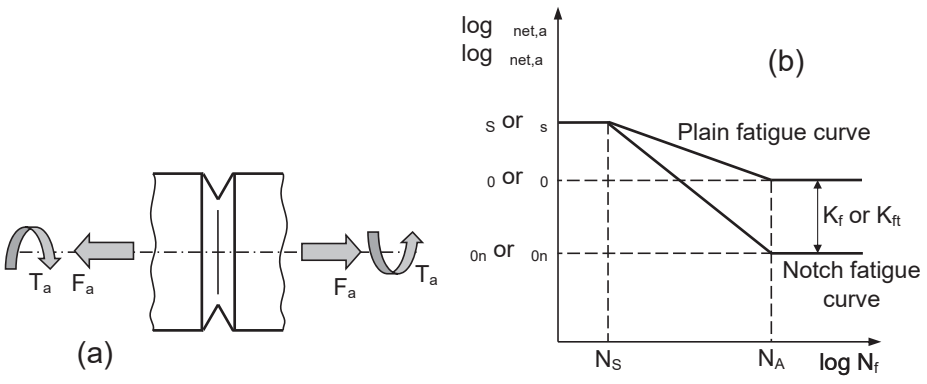

Fig. 1. Notched shaft subjected to either cyclic axial loading or cyclic torsion (a); plain and notch fatigue curve and definition of fatigue strength reduction factors K_f and K_{ft} (b).

refined meshes, where the mesh density must increase as the notch being designed becomes sharper and sharper. Since the computational time increases as the number of elements increases, performing the fatigue assessment using local approaches can result in calculation times that are not compatible with the industrial needs in terms of product development life cycle.

As far as standard geometries are concerned, the above problems can somehow be overcome by performing the fatigue assessment in terms of nominal stresses used along with suitable fatigue strength reduction factors [23-25]. This design methodology is so simple that, unsurprisingly, it was adopted also by Gough back in the 1940s to post-process the fatigue results he generated by testing notched metallic shafts under in-phase bending and torsion [26].

In this setting, it is interesting to point out that, nowadays, nominal stresses are still used in situations of practical interest to perform the fatigue assessment of welded components. This explain why the use of the nominal stress-based approach is recommended by a number of standards and recommendations specifically dealing with the problem of designing welds against fatigue – see, for instance, Refs [20,27-29].

Given the fatigue design scenario briefly sketched above, the aim of the present paper is to assess the accuracy and reliability of the Modified Wöhler Curve Method (MWCM) [30,31] when fatigue damage is quantified according to the nominal stress-based approach. This systematic validation exercise will be based on a large number of experimental results taken from the literature and generated by testing, under CA/VA tension/torsion, metallic specimens containing different geometrical features.

2. Nominal stress-based approach and fatigue strength reduction factors

In order to understand how the nominal stress-based approach works, consider the notched cylindrical shaft shown in Fig. 1a. Assume that this notched bar is subjected either to a cyclic axial force or to a cyclic torsional moment. The axial force and the applied torque have amplitude equal to F_a and T_a, respectively, and the associated nominal stress amplitudes are to be calculated with respect to the net cross-sectional area [25].

Consider now the Wöhler log–log diagram (or the SN log–log diagram) shown in Fig. 1b where two different fatigue curves are plotted. The upper fatigue curve is the one generated by testing (under either axial loading or torsion) plain specimens of a given material. The lower fatigue curve is instead the one determined by testing specimens made of the same material and weakened by a known geometrical feature. In plain specimens, obviously, the net nominal stresses coincide with the actual streses being applied to the material. This is why the schematic Wöhler diagram of Fig. 1b that plots the amplitude of the nominal net stresses (i.e., either $\sigma_{net,a}$ or $\tau_{net,a}$) against the number of cycles to failure can be used to display consistently both the plain and the notch fatigue curve. As per Fig. 1b, the detrimental effect of the considered notch under axial (or bending) loading and under torsion is quantified via fatigue strength reduction factor K_f and K_{ft}, respectively, as follows [24,25,32]:

$$K_f = \frac{\sigma_0}{\sigma_{0n}} \tag{1}$$

$$K_{ft} = \frac{\tau_0}{\tau_{0n}} \tag{2}$$

In definitions (1) and (2) σ_0 and τ_0 are the plain material fatigue limits, whereas σ_{0n} and τ_{0n} are the corresponding notch fatigue limits. To determine K_f and K_{ft} in a consistent way, the plain and notch fatigue limits used in Eqs (1) and (2) are recommended to be determined either under the same load ratio or by imposing the same mean stress value.

As to the validity of definitions (1) and (2), another important aspect that is worth pointing out here is that K_f and K_{ft} can be determined not only through plain and notch fatigue limits, but also through plain and notch endurance limits.

As far as metallic materials are concerned, the *fatigue limit* is defined as that specific stress level which results in the formation of non-propagating cracks whose propagation is arrested either by the first grain boundary or by the first micro-structural barrier [33,34]. As a matter of fact, in situations of practical interest fatigue limits are seen to disappear due to the effect of transitory cyclic-dependent and time-dependent mechanisms/processes (including profile and characteristics of the real loading history and environmental conditions) [35,36]. As a consequence of these mechanisms/processes, the crack initiation locations are transferred from the surface of the components to the internal bulk material, with these internal cracks eventually governing the whole fatigue failure process [35].

To overcome the problem associated with the determination of the fatigue limit and its potential elimination, it is common practise to define a reference strength in the high-cycle fatigue regime which is termed the *endurance limit*. By definition the endurance limit is the stress level (either amplitude or range) extrapolated at a given number of cycles to failure. Typically, the reference number of cycles to failure used to determine the endurance limit ranges between $5{\cdot}10^5$ up 10^8 cycles to failure [25,32].

Having highlighted the differences between fatigue and endurance limit, the considerations summarised in the present section will be based solely on fatigue limits. This is because the knowledge reviewed in this section was originally developed in terms of fatigue limits. However, the same ideas and tools remains valid also when the fatigue strength reduction factors are determined in terms of endurance limits. This holds true as long as the plain and notch endurance limits used in definitions (1) and (2) are determined under the same experimental conditions and extrapolated at the same reference number of cycles to failure, N_A [25].

Definitions (1) and (2) together with Fig. 1b make it clear that the experimental approach represents the most accurate and reliable way to determine the fatigue strength reduction factors. However, since in situations of industrial interest this is not always feasible, systematic theoretical and experimental work has been done since about the middle of the last century to derive specific formulas suitable for estimating K_f and K_{ft} for different materials and different geometrical features [25,37,38].

In order to understand the way the empirical formulas suitable for estimating K_f and K_{ft} work in practise, it can be recalled here that, according to Peterson [24], the fatigue strength reduction factor depends on both the notch sensitivity factor, q, and the corresponding linear-elastic stress concentration factor as follows:

$$K_f = 1 + q(K_t - 1) \tag{3}$$

$$K_{ft} = 1 + q(K_{tt} - 1) \tag{4}$$

In Eq. (3) K_t is the net stress concentration factor under uniaxial loading (i.e., under either tension or bending), whereas in Eq. (4) K_{tt} is the net stress concentration factor under torsion.

As per definitions (3) and (4), q ranges between 0 and 1. In particular, when q is equal to zero the presence of the notch does not lower the plain fatigue limit. In contrast, when q is equal to unity, K_f becomes equal to K_t and the fatigue assessment is done directly in terms of linear-elastic peak stresses.

As far as structural steels are concerned, according to Peterson [24], Eqs (3) and (4) can be rewritten as follows [32]:

$$K_f = 1 + \frac{K_t - 1}{1 + \frac{a_p}{r_n}} \tag{5}$$

$$K_{ft} = 1 + \frac{K_{tt} - 1}{1 + \frac{a_{pt}}{r_n}} \tag{6}$$

where material characteristic lengths a_p and a_{pt} can be estimate (for

$\sigma_{UTS} > 560$ MPa) as [32]:

$$a_P = 0.0254\left(\frac{2079}{\sigma_{UTS}}\right)^{1.8} [mm] \quad (7)$$

$$a_{Pt} = 0.01524\left(\frac{2079}{\sigma_{UTS}}\right)^{1.8} [mm] \quad (8)$$

In Eqs. (7) and (8), the material ultimate tensile strength, σ_{UTS}, is measured in units of MPa.

As far as notched components made of aluminium are concerned, constants a_P and a_{Pt} can be assumed to be invariably equal to 0.635 mm [39].

Turning to cast iron, Heywood [40] proposed the following relationship to estimate the fatigue strength reduction factor under uniaxial fatigue loading:

$$K_f = \frac{K_t}{1 + 2\frac{\sqrt{a_H}}{\sqrt{r_n}}\left(\frac{K_t - 1}{K_t}\right)} \quad (9)$$

where.

$$\sqrt{a_H} = \frac{173.6}{\sigma_{UTS}} [mm\ 1/2] \ for\ cast\ iron\ with\ spheroid\ graphite \quad (10)$$

$$\sqrt{a_H} = 0.605 [mm 1/2] \ for\ cast\ iron\ with\ flake\ graphite \quad (11)$$

Eq. (9) together with Eqs. (10) and (11) can also be used to estimate K_{ft}, with this being done by simply replacing K_t with K_{tt} in Eq. (9).

Having estimated K_f and K_{ft} for the specific geometrical feature being designed, the associated fatigue curve can be derived as shown in Fig. 1b. In particular, if the fatigue strength of the un-notched material is known from the experiments, then the assumption can be made that both the notch and the plain fatigue curve have their knee points at the same number of cycles to failure, N_A (Fig. 1b). In contrast, if the position of the plain fatigue curve's knee point is not known, then either a suitable value for N_A can be chosen according to Sonsino's recommendations [36] or N_A can be taken invariably equal to $2{\cdot}10^6$ cycles to failure as suggested by Atzori [42].

Having defined a suitable endurance/fatigue limit at a given number of cycles to failure, N_A, the subsequent step is to define a second reference point in the low-cycle fatigue regime - i.e., at N_S cycles to failure (see Fig. 1b). As far as metals are concerned, N_S is seen to be different for different materials and different load ratios. Its value ranges in the interval $1/4–10^4$ cycles to failure [32], with 10^3 cycles to failure being a reliable value recommended to be used to estimate N_S in situations of practical interest [42]. Having chosen a suitable value for N_S, it is possible to conclude by observing that, for a given material, the value of the amplitude of the stress at N_S cycles to failure varies as the load ratio (or the mean stress) increases [25].

As mentioned earlier, examination of the state of the art shows that, since the middle of the last century to date, a number of empirical formulas has been proposed to estimate the fatigue strength reduction factors in situations of practical interest. The specific empirical equations reviewed in the present section will be used in Section 5 to check the accuracy of the MWCM when this design method is calibrated through axial and torsional fully-reversed notch fatigue curves that are estimated. For a more complete and exhaustive overview of those formula suitable for deriving K_f with K_{ft}, the reader is referred to those books and scientific articles specifically addressing this problem in depth – see, for instance, Refs [25,32,37-41] and references reported therein.

To conclude the present section, it is worth pointing out that, as far as multiaxial load histories are concerned, by its nature, the nominal stress-based approach is not always able to locate unambiguously the position of the crack initiation locations. In particular, as observed, for instance, by Gough [26] when commenting the results he generated by testing splined shafts under in-phase bending and torsion, the position of the critical locations may change as the degree of multiaxiality of the load history varies. This can clearly result in a certain level of inaccuracy, forcing some simplifying assumptions to be made in order to be able to design complex stress concentrators against multiaxial fatigue [22,25]. It is interesting to observe that this problem can be encountered also when the nominal-stress based approach is used to perform the fatigue assessment of welded joints [25,43]. This limitation is intrinsic in the nature of nominal stresses and can affect the accuracy of any multiaxial fatigue design approach when applied in conjunction with this simplified stress analysis strategy. Clearly, as any other criterion, the MWCM as well is affected by this problem when applied in terms of nominal stresses. However, these limitations can be overcome by simply using this approach along with the Theory of Critical Distances [8-10,14].

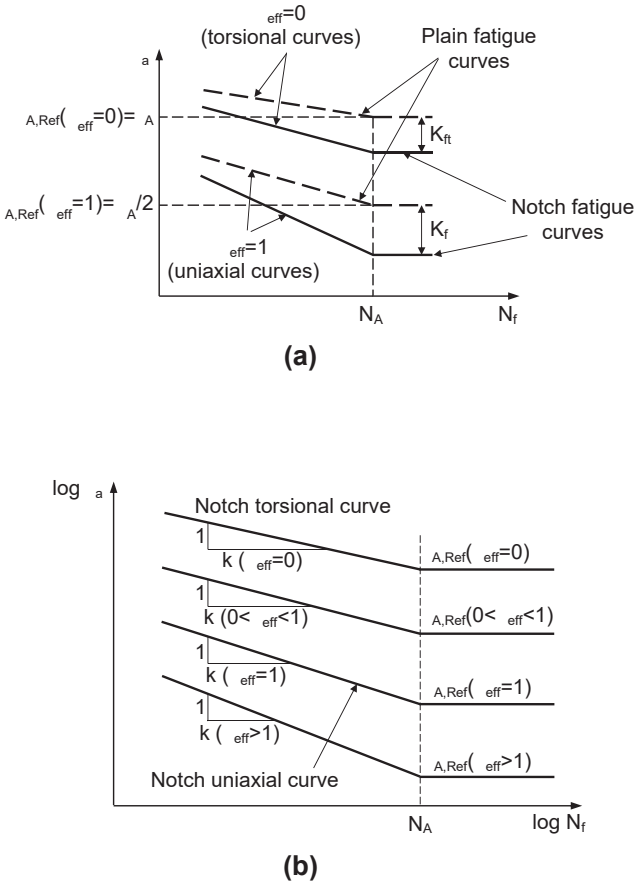

Fig. 2. Modified Wöhler diagrams plotted in terms of nominal net stresses.

Having briefly reviewed key features and limitations of the nominal stress-based approach, in the next sections this stress analysis strategy will be used in conjunction with the MWCM to formulate a simplified design methodology suitable for designing notched components against CA and VA multiaxial load histories.

3. Modified Wöhler diagram, nominal stresses and fatigue strength reduction factors

The MWCM estimates fatigue damage through the shear and normal stress components relative to the plane of maximum shear stress amplitude (i.e., relative to the so-called *critical plane*). The definitions recommended to be used to determine the stress components relative to the critical plane will be reviewed in Section 4 in great detail.

The way the MWCM performs fatigue assessment can be visualised via the modified Wöhler diagrams reported in Fig. 2, with these log–log charts plotting the shear stress amplitude relative to the critical plane, τ_a, against the number of cycles to failure, N_f. The shear stress amplitude

used in the modified Wöhler diagrams of Fig. 2 is assumed to be calculated by referring to the nominal net section. Since, as already recalled earlier, in un-notched components, the nominal net stresses coincide with the actual, real stresses damaging the material being designed, both plain and notch fatigue curves can consistently be plotted together in modified Wöhler diagrams as schematically shown in Fig. 2a.

The MWCM assesses fatigue damage via the following critical plane stress ratio [25,44]:

$$\rho_{eff} = \frac{m \bullet \sigma_{n,m} + \sigma_{n,a}}{\tau_a} \tag{12}$$

where $\sigma_{n,m}$ and $\sigma_{n,a}$ are mean value and the amplitude of the stress component perpendicular to the critical plane, respectively. Constant m (that ranges between zero and unity) quantifies the material sensitivity to the presence of superimposed static stresses and can be determined by running appropriate experiments [25,44]. Stress ratio ρ_{eff} is seen to be sensitive not only to the presence of non-zero mean stresses, but also to the degree of multiaxiality and non-proportionality of the load history being assessed [25]. For instance, the use of definition (12) results in a ρ_{eff} value equal to unity under fully-reversed uniaxial fatigue loading, whereas ρ_{eff} is invariably equal to zero under cyclic torsion.

For a given material, the fully-reversed uniaxial and torsional plain fatigue curves can be plotted in the modified Wöhler diagram by observing that the corresponding negative inverse slopes (i.e., k and k_0, respectively) remain un-changed, whereas the associated endurance limits can directly be rewritten as follows [30,31]:

$$\tau_{A,Ref}\left(\rho_{eff}=1\right) = \frac{\sigma_A}{2} \tag{13}$$

$$\tau_{A,Ref}\left(\rho_{eff}=0\right) = \tau_A \tag{14}$$

In definitions (13) and (14) σ_A and τ_A are used to denote the uniaxial and torsional plain endurance limits, respectively, with these endurance limits being extrapolated at a reference number of cycles to failure equal to N_A.

As schematically shown in Fig. 2a, much experimental evidence [25,30,31] suggests that in modified Wöhler diagrams the torsional fatigue curve ($\rho_{eff}=0$) is above the uniaxial fatigue curve ($\rho_{eff}=1$), with the validity of this schematisation being fully supported also by von Mises' strength criterion [30].

Turning to the notch fatigue problem, Fig. 2a visualises the way the fatigue strength reduction factors can be used in Modified Wöhler diagrams to link the uniaxial and torsional notch fatigue curves to the corresponding plain ones. In particular, as per Fig. 2a, K_f and K_{ft} can directly be rewritten as follows [25,30,31]:

$$K_f = K_f\left(\rho_{eff}=1\right) = \frac{\sigma_A/2}{\sigma_{An}/2} = \frac{\sigma_A}{\sigma_{An}} \tag{15}$$

$$K_{ft} = K_f\left(\rho_{eff}=0\right) = \frac{\tau_A}{\tau_{An}} \tag{16}$$

where σ_{An} and τ_{An} are the net nominal stress notch endurance limits extrapolated at N_A cycles to failure under uniaxial and torsional fatigue loading, respectively.

Based on the reasoning summarised above, the Modified Wöhler diagram of Fig. 2a suggests that, for a given material, $\tau_{A,Ref}(\rho_{eff})$ decreases as stress ratio ρ_{eff} increases, with this leading to the schematization seen in Fig. 2b. In other words, according to the Modified Wöhler diagram of Fig. 2b, the MWCM postulates that fatigue damage increases as ρ_{eff} increases, with this holding true not only for plain materials, but also for notched components. Since in situations of practical interest the available fatigue curves are those generated under uniaxial and torsional fully-reversed fatigue loading, the modified Wöhler curves characterised by a value of ρ_{eff} different either from zero (torsion) or from unity (uniaxial case) must be somehow estimated. This can be done by observing that the k_τ vs. ρ_{eff} function as well as the $\tau_{A,Ref}$ vs. ρ_{eff} function can be expressed by using simple linear laws [25,30,31]:

$$k_\tau\left(\rho_{eff}\right) = (k-k_0) \bullet \rho_{eff} + k_0 \tag{17}$$

$$\tau_{A,Ref}\left(\rho_{eff}\right) = \left(\frac{\sigma_{An}}{2} - \tau_{An}\right) \bullet \rho_{eff} + \tau_{An} \tag{18}$$

In Eq. (17) k_τ (ρ_{eff}) is used to denote the negative inverse slope of the notch modified Wöhler curves, with k and k_0 being the negative inverse slope of the uniaxial and torsional notch fatigue curve, respectively. Relationships (17) and (18) make it evident that, being simple linear equations, the constants in the MWCM calibration functions can directly be calculated from the uniaxial and torsional fully-reversed fatigue curves.

The next sub-sections will explain the procedures being recommended to be followed to employ the MWCM to estimate fatigue lifetime of notched components subjected to both CA and VA multiaxial fatigue loading. However, before considering these design methodologies in detail, it is important to recall here that governing equations (17) and (18) should be used as long as ρ_{eff} is lower than a specific threshold value, ρ_{lim}, that can be estimated as follows [25,44]:

$$\rho_{lim} = \frac{\tau_{An}}{2\tau_{An} - \sigma_{An}} \tag{19}$$

In contrast, when ρ_{eff} is larger than ρ_{lim}, the modified Wöhler curve to be used to assess fatigue damage is recommended to be derived from Eqs (17) and (18) by setting ρ_{eff} invariably equal to ρ_{lim} [25,45]. This correction was introduced to take into account the fact that under large values of stress ratio ρ_{eff} - i.e., when $(m \bullet \sigma_{n,m} + \sigma_{n,a}) \gg \tau_a$ in definition (12) - fatigue damage is no longer governed solely by the shear stress. Accordingly, under these circumstances, the conventional critical plane approach must be somehow adjusted so that the change in the physical mechanisms leading to final breakage [45,46] can be taken into account and modelled effectively.

The reasoning behind the introduction of threshold ratio (19) can be explained [44] by referring to the classic damage model formulated by Socie [47]. In particular, as per this physical model, Stage 1 cracks initiate on those planes that are characterised by the maximum amplitude of the shear stress [47]. Further, the extent of fatigue damage is a function also of the stress perpendicular to the critical plane. From a physical viewpoint, this is a consequence of the fact that, by opening the micro/meso-cracks, tensile normal stresses tend to facilitate their growth. In contrast, compressive normal stresses have a propensity to slow down the propagation process as a consequence of an increase in the level of friction between the surfaces of the micro/meso-cracks. In this setting, by running a comprehensive experimental investigation, Kaufman and Topper [48] demonstrated that a further increment in the normal mean stress does not lead to a further increase of the associated extent of fatigue damage as soon as the mean stress perpendicular to the critical plane becomes larger than a specific material threshold value. Kaufman and Topper explained this experimental evidence by observing that under very large values of the mean stress perpendicular to the critical plane, micro/meso cracks are already fully open so that the shearing forces are directly transferred to the crack tips. This supports a Mode II-governed growth. In contrast, if the mean stress perpendicular to the critical plane is lower than the above material threshold, the interactions between the crack faces prevent the shearing forces from being fully transmitted to the crack tips. This situation results in a decrease of the fatigue damage extent as a consequence of the fact that the crack propagation process is retarded by the friction acting between the faces of the micro/meso cracks. According to the considerations briefly summarised above, this threshold value for the normal mean stress can be thought of as a material property as a consequence of the fact that the morphology of the crack surfaces is different for different materials, with this leading to different levels of interference/friction for a given magnitude of the stress perpendicular to the critical plane. From a multiaxial fatigue design point of view, these physical processes

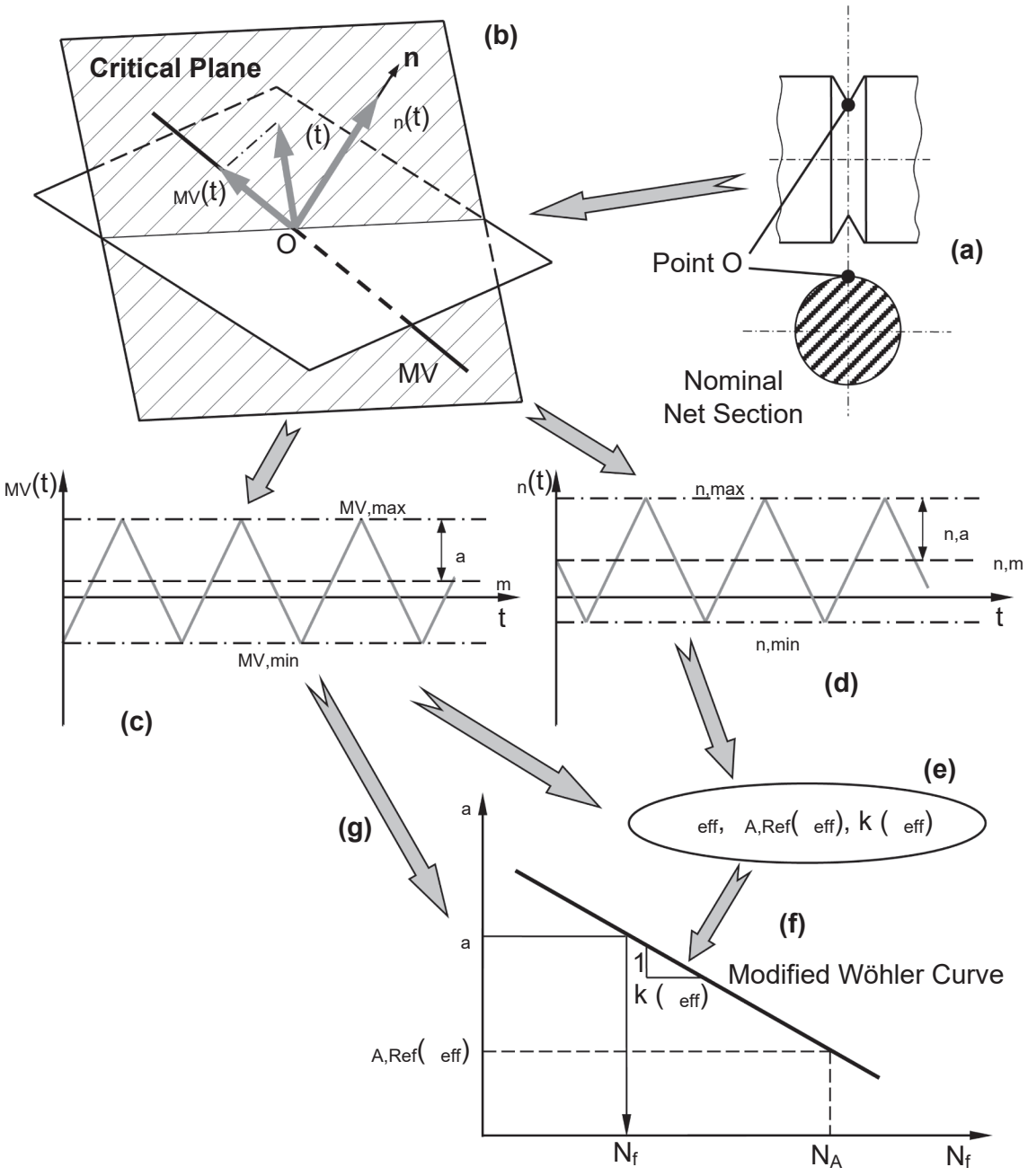

Fig. 3. The MWCM applied along with the nominal stress-based approach to design notched components against CA multiaxial fatigue loading.

observed and discussed by Kaufmann and Topper [48] are incorporated into the MWCM by simply taking ρ_{eff} equal to ρ_{lim} when $\rho_{eff} > \rho_{lim}$ [25,45].

Having summarised the reasoning leading to the definition of ρ_{lim}, Eq. (19), it is possible to conclude by recalling that, given the way they are defined and calculated, nominal stress are poorly related with the actual distributions of the stresses damaging the material regions in the vicinity of the notch tips. This is the reason why, under particular circumstances, the use of Eq. (19) can result in ρ_{lim} values that are lower than unity. To overcome this limitation that has to be ascribed simply to the fact that, in practice, nominal stresses are nothing but fictitious design quantities, ρ_{lim} can be taken invariably equal to unity when Eq. (19) returns ρ_{lim} values lower than unity.

4. The MWCM applied in conjunction with the nominal stress-based approach

4.1. Design against CA multiaxial fatigue loading

The schematic flowchart reported in Fig. 3 summarises the design procedure to be followed to use the MWCM along with nominal stresses to design notched components against CA multiaxial fatigue.

Given the geometry of the notched component being designed, the stress analysis is performed in terms of nominal net stresses calculated at the assumed critical point (point O in Fig. 3a). The stress state at the critical point is then post-processed according to the Shear Stress-Maximum Variance Method (τ-MVM) [49-52] to determine the orientation of the critical plane. As postulated by the τ-MVM, the critical plane is defined as the plane containing that direction (direction MV in Fig. 3b) experiencing the maximum variance of resolved shear stress

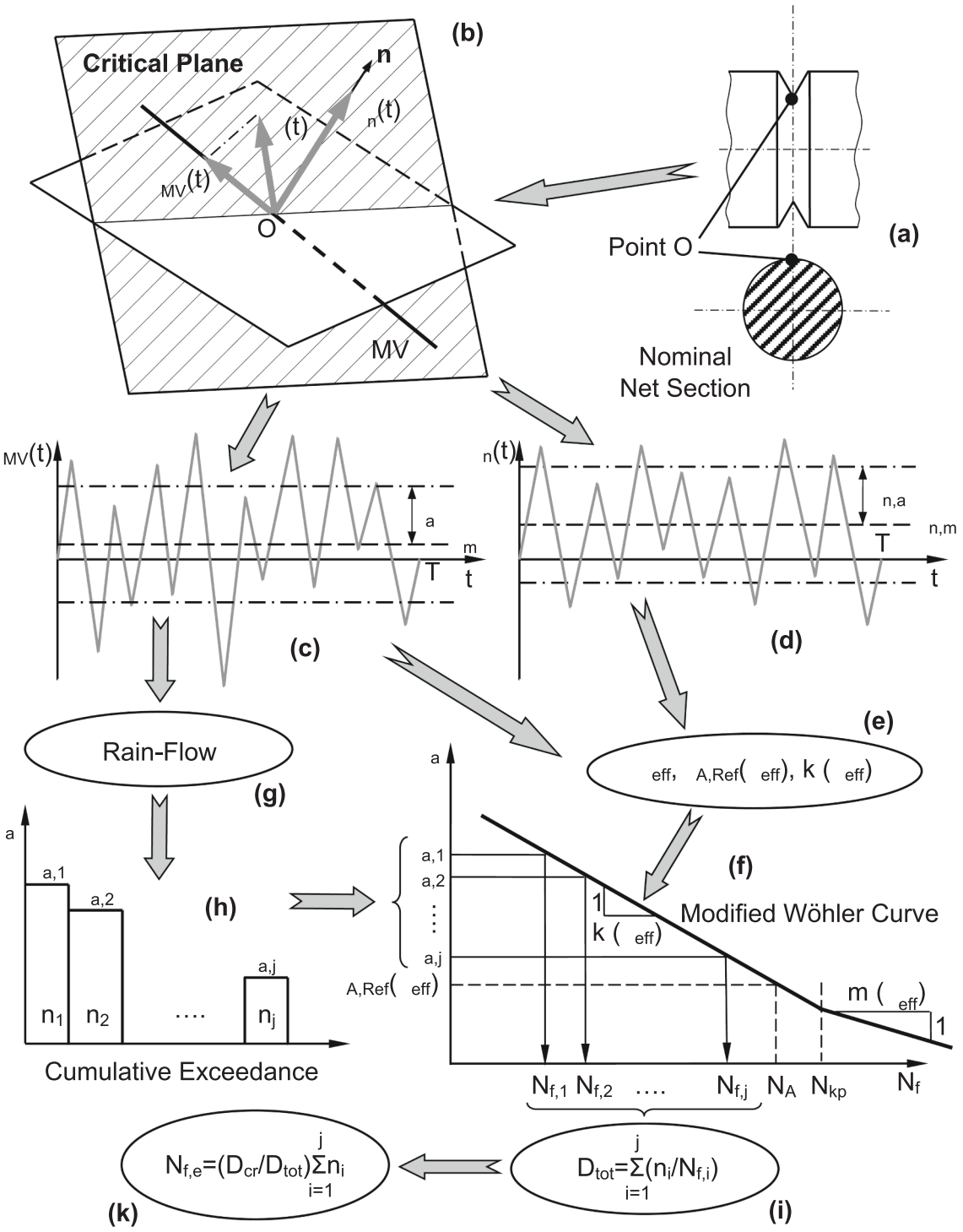

Fig. 4. The MWCM applied along with the nominal stress-based approach to design notched components against VA multiaxial fatigue loading.

$\tau_{MV}(t)$. In Fig. 3b $\tau(t)$ is the instantaneous value of the shear stress relative to the material plane under investigation, whereas $\tau_{MV}(t)$ is the instantaneous value of $\tau(t)$ resolved along direction MV. As soon as the orientation of the critical plane is known, it is straight forward to determine the direction perpendicular to this plane and then the associated normal stress, $\sigma_n(t)$ – see Fig. 3b.

Since CA signals $\tau_{MV}(t)$ and $\sigma_n(t)$ are both monodimensional time-variable stress quantities, they can be post-process directly to determine the associated amplitudes and mean values via the following standard definitions (Fig. 3c and 3d):

$$\tau_a = \frac{\tau_{MV,max} - \tau_{MV,min}}{2}; \tau_m = \frac{\tau_{MV,max} + \tau_{MV,min}}{2} \tag{20}$$

$$\sigma_{n,a} = \frac{\sigma_{n,max} - \sigma_{n,min}}{2}; \sigma_{n,m} = \frac{\sigma_{n,max} + \sigma_{n,min}}{2} \tag{21}$$

As soon as the necessary stress components relative to the critical plane are known, ratio ρ_{eff} can be calculated directly through definition (12). Subsequently, ratio ρ_{eff} is used together with calibration functions (17) and (18) to estimate the pertinent modified Wöhler curve to be used to assess fatigue damage (Fig. 3e and 3f). Finally, the shear stress

amplitude relative to the critical plane, τ_a, is used to estimate the number of cycles to failure, $N_{f,e}$, through the following standard power law (Fig. 3g and 3f) [25]:

$$N_{f,e} = N_A \bullet \left[\frac{\tau_{A,Ref}\left(\rho_{eff}\right)}{\tau_a}\right]^{k_\tau\left(\rho_{eff}\right)} \tag{22}$$

The CA solution presented in this section allows us to discuss briefly also the most relevant difference in terms of *modus operandi* between the MWCM and other classic critical plane approaches - such as, for instance, Fatemi & Socie's criterion [53], the multiaxial formulation of the SWT parameter [54], and Wang & Brown's method [55]. In particular, initially the classic fatigue life estimation techniques all calculate a specific damage parameter by combining (in different ways) the stress/strain components relative to the critical plane. Subsequently, fatigue lifetime is assessed by directly using the damage parameter being estimated along with either the uniaxial or the torsional fatigue curve. In other words, the core idea behind the classic critical plane approaches is that lifetime under multiaxial fatigue loading is predicted by bringing the design problem back to either the uniaxial or the torsional case, with this holding true independently of the degree of multiaxiality and non-proportionality of the load history being assessed. In contrast, according to Fig. 2b and 3f, the MWCM performs the fatigue assessment by directly referring to a design curve which is estimated, via stress ratio ρ_{eff} – Eq.(12), by considering the actual degree of multiaxiality and non-proportionality characterising the relevant time-variable state of stress being post-processed.

Having highlighted this key philosophical difference, in the next section the use of the MWCM will be extended to VA multiaxial fatigue situations.

4.2. Design against VA multiaxial fatigue loading

The schematic flowchart reported in Fig. 4 shows the different steps that need to be taken in order to use the MWCM in conjunction with nominal stresses to estimate fatigue lifetime of notched components subjected to VA multiaxial load histories.

As done for the CA case, initially the relevant stress tensor at the point of interest (point O in Fig. 4a) has to be calculated in terms of nominal net stresses. This stress tensor is then post-processed to determine the orientation of the critical plane. As postulated by the τ-MVM [49-52], the critical plane is again defined as the plane containing that direction experiencing the maximum variance of resolved shear stress $\tau_{MV}(t)$ - i.e. direction MV in Fig. 4b. Given the orientation of the critical plane, the direction normal to this plane is used to determine stress component $\sigma_n(t)$ - see Fig. 4b.

Subsequently, VA stress signals $\tau_{MV}(t)$ and $\sigma_n(t)$ are post-processed to calculate the associated equivalent amplitudes and mean values (Fig. 4c and 4d), with this being done by taking full advantage of the following definitions [14,56,57]:

$$\tau_m = \frac{1}{T}\int_0^T \tau_{MV}(t) \bullet dt \tag{23}$$

$$\tau_a = \sqrt{2 \bullet Var[\tau_{MV}(t)]} \ \ where \ \ Var[\tau_{MV}(t)] = \frac{1}{T}\int_0^T \left[\tau_{MV}(t) - \tau_m\right]^2 \bullet dt \tag{24}$$

$$\sigma_{n,m} = \frac{1}{T}\int_0^T \sigma_n(t) \bullet dt \tag{25}$$

$$\sigma_{n,a} = \sqrt{2 \bullet Var[\sigma_n(t)]} \ \ where \ \ Var[\sigma_n(t)] = \frac{1}{T}\int_0^T \left[\sigma_n(t) - \sigma_{n,m}\right]^2 \bullet dt \tag{26}$$

The stress components relative to the critical plane quantified according to definitions (23) to (26) can now be used together with Eq. (12) to determine stress ratio ρ_{eff}. Ratio ρ_{eff} is then employed along with calibration functions (17) and (18) to estimate the modified Wöhler curve suitable for quantifying the extent of damage associated with the VA multiaxial load history under investigation (Fig. 4e and 4f).

Having derived the pertinent modified Wöhler curve, this curve has to be adjusted so that the damage associated with the stress cycles of low stress amplitude can be quantified correctly [58]. In particular, as recommended by Haibach [59], the negative inverse slope in the high-cycle fatigue regime (i.e., for $N_f > N_{kp}$ in Fig. 4f) is suggested to be corrected as follows:

$$m_\tau\left(\rho_{eff}\right) = 2 \bullet k_\tau\left(\rho_{eff}\right) - 1 \tag{27}$$

where negative slope (27) is calculated by taking $\rho_{eff} = \rho_{lim}$ when $\rho_{eff} > \rho_{lim}$. Further, if the position of the knee point (N_{kp} in Fig. 4f) is not known from the experiments, N_{kp} can be estimated by taking full advantage of the available recommendations [36] see also Fig. 4f.

Having corrected the modified Wöhler curve to be used to assess damage under VA loading (Fig. 4f), the subsequent step (Fig. 4c and 4g) is to take full advantage of the standard Rain-Flow method [60] to post-process stress signal $\tau_{MV}(t)$. By so doing, the resolved shear stress cycles being counted can be used to build the associated load spectrum (Fig. 4h). It is important to highlight that, in this theoretical setting, the Rain-Flow method can be employed in a rigorous way [60] since, by definition, signal $\tau_{MV}(t)$ is a monodimensional time-variable stress quantity.

The final step in the VA design process involves the use of the determined shear stress spectrum together with the pertinent modified Wöhler curve to quantify the extent of damage associated with any shear stress cycles being counted (Fig. 4h and 4f). In particular, having determined $N_{f,i}$ – via Eq. (22) - for any shear stress level $\tau_{a,i}$, the number of cycles to failure can directly be estimated as follows (Fig. 4i and 4k):

$$D_{tot} = \sum_{i=1}^{j} \frac{n_i}{N_{f,i}} \tag{28}$$

$$N_{f,e} = \frac{D_{cr}}{D_{tot}} \sum_{i=1}^{j} n_i \tag{29}$$

In Eq. (29), D_{cr} is the critical value of damage sum D_{tot} that results in the fatigue breakage of the notched structural component being assessed. It is important to point out that D_{cr} can be taken invariably equal to unity according to the classic theory due to Palmgren [61] and Miner [62]. However, much experimental evidence suggests that, in situations of practical interest, D_{cr} varies in the range 0.02–5, with its average value being equal to 0.27 for steel components and to 0.37 for aluminium components [58].

An interesting example highlighting the problems behind an accurate determination of D_{cr} is represented by the steel welded joints tested by Sonsino and Kueppers [63]. In particular, from the results generated by testing tube-to-plate welded joints under Gaussian Spectra with sequence length equal to $5{\cdot}10^4$ cycles, they observed that for their connections the critical value of the damage sum was equal to 0.08 under VA pure bending, to 0.38 under VA pure torsion, to 0.35 under in-phase VA bending and torsion, and to 0.38 under 90° out-of-phase VA bending and torsion. This explains the reason why, as far as welded joints are concerned, the IIW [20] recommends to set D_{cr} equal to 0.5, with this value being suggested by observing that *"for spectra with high mean stress fluctuations, the damage sum may be even lower,* i.e. $D = 0.2$*"*. Similarly, the FKM-Guideline [64] recommends to design structural components of cast aluminium by taking the value of the critical damage sum equal to 0.3.

The considerations briefly reported above make it evident that, for a given metallic material, the critical value of the damage sum is seen to

Table 1
Summary of the calibration fatigue curves determined from experimental results generated by testing notched specimens (Fig. 5) under axial loading and torsion.

Material	Ref.	d_n	d_g	r_n	α	Uniaxial Loading				Torsional Loading			
						R	σ_{An} [1]	k	Tσ	R	τ_{An} [1]	k_0	Tτ
		[mm]	[mm]	[mm]	[°]		[MPa]				[MPa]		
C40 Steel (1)	[65]	12	20	0.5	90	−1	117.8	4.6	1.350	−1	152.8	8.2	1.360
En3B	[10]	5	8	0.2	60	−1	85.0	3.5	1.961	−1	154.4	7.7	1.435
SAE 1045	[66]	40	50	5.0	–	−1	188.6	6.3	1.216	−1	156.6	12.5	1.148
Low Carbon Steel	[67]	7.62	12.7	0.2	35	−1	66.9	3.8	1.662	−1	122.9	9.9	1.274
		7.62	12.7	0.4	35	−1	95.3	6.0	1.303	−1	156.4	16.9	1.099
39NiCrMo3	[68]	12	20	0.1	90	−1	157.1	4.9	1.361	−1	305.8	15.6	1.254
AISI 416	[11]	12	20	0.1	90	−1	97.5	3.6	1.882	−1	218.6	12.2	1.269
		16	20	0.1	90	−1	95.1	4.0	1.438	−1	221.3	14.5	1.139
		19	20	0.1	90	−1	181.6	7.2	1.155	−1	201.6	13.3	1.074
EN-GJS400	[69,70]	12	20	0.1	90	−1	84.0	5.4	1.534	−1	151.4	13.1	1.147
40CrMoV13.9	[75]	12	20	0.1	90	−1	239.9	8.5	1.334	−1	271.4	13.3	1.143
2024-T3	[71]	25.4	29	1.6	–	−1	90.4	11.6	1.097	−1	55.0	6.9	1.111
Al 7050-T7451	[73]	10	15	0.1	60	−1	53.2	5.7	2.629	−1	96.3	4.8	1.989

[1] Endurance limits extrapolated at $N_A = 2 \bullet 10^6$ cycles to failure.

Table 2
Static properties and plain fatigue curves generated under axial and torsional loading used to estimate the calibration notch fatigue curves reported in Table 4.

Material	Ref.	σ_Y	σ_{UTS}	Uniaxial Loading				Torsional Loading				m
				R	σ_A [1]	k	T_σ	R	τ_A [1]	k_0	Tτ	
		[MPa]	[MPa]		[MPa]				[MPa]			
C40 Steel (1)	[65]	537	715	−1	264.2	17.1	1.171	−1	195.8	18.2	1.087	1
En3B	[10]	653	676	−1	333.9	19.7	1.105	−1	258.5	18.7	1.205	0.2
SAE 1045	[66]	380	621	−1	195.8	9.0	1.148	−1	115.8	10.2	1.147	–
Low Carbon Steel	[67]	312	500	−1	216.2	15.2	1.185	−1	187.1	22.8	1.064	–
39NiCrMo3	[68]	900	995	−1	315.4	7.2	1.259	−1	265.3	9.5	1.179	1
AISI 416 steel	[11]	570	700	−1	349.6	29.8	1.067	−1	225.4	16.6	1.207	1
EN-GJS400	[69,70]	267	378	−1	142.2	12.9	1.388	−1	137.6	10.1	1.158	0.4
2024-T3	[71,72]	330	495	−1	157.7	7.1	1.339	−1	129.4	10.5	1.281	–
Al 7050-T7451	[73]	404	488	−1	106.3	5.9	2.200	−1	85.7	4.9	1.499	–
C40 Steel (2)	[14]	672	852	−1	272.1	9.4	1.211	−1	219.5	12.8	1.297	0.19
En8	[17]	453	701	−1	171.3	9.3	1.122	−1	157.9	13.4	1.219	–
AISI 316 L	[74]	380	642	−1	249.0	15.3	1.147	−1	216.1	32.7	1.062	0.53

[1] Endurance limits extrapolated at $N_A = 2 \bullet 10^6$ cycles to failure.

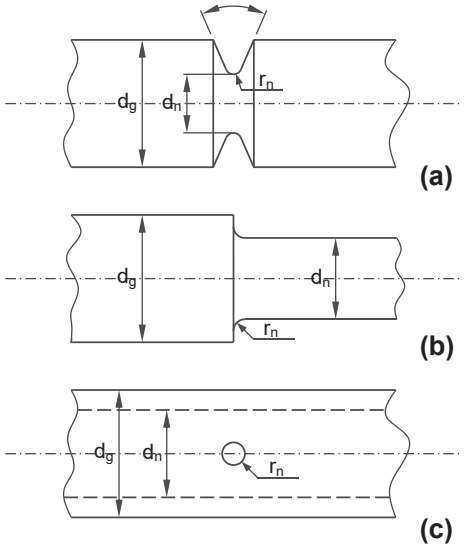

Fig. 5. Geometries of the considered notched specimens.

depend not only on characteristics and degree of multiaxiality/non-proportionality of the VA load history being considered, but also on the geometry of the assessed component. In this setting, it is possible to conclude by observing that, while there are some design guidelines (such as, for instance, Refs [63,64]) allowing a reference value for the critical value of the damage sum to be somehow selected, still the most accurate way to determine D_{cr} is by running appropriate experiments.

5. Accuracy against experimental notch fatigue results

To check the accuracy and reliability of the MWCM when this criterion is applied in terms of nominal stresses, a systematic literature survey was carried out in order to select suitable experimental data sets. The validation exercise summarised in the present section involved 14 different metallic materials (see Tables 1 and 2).

The notched cylindrical specimens with fillet of SAE 1045 [66] were tested under combined bending and torsion. In contrast, the other data being considered in this investigation were all generated under combined axial loading and torsion, with the laboratory specimens being tested under both constant and variable amplitude load histories. The effect of both superimposed static stresses and loading path's degree of non-proportionality was assessed systematically. The experimental studies being considered were based on three different types of specimens. The cylindrical specimens contained circumferential notches characterised by different values of depth, root radius and opening angle (Fig. 5a and 5b). In contrast, the thin-walled tubular specimens were weakened by a through-thickness hole (Fig. 5c).

The notched specimens of C40 steel [65] were normalised, with this process resulting in two micro-structural phases, i.e., ferrite and pearlite. Further, as a consequence of the drawing process, the two phases had their main direction parallel to the longitudinal axis of the specimens. The tests were run at a frequency ranging in the interval 5–20 Hz. Under

Table 3
Stress concentration factors and experimental/estimated fatigue strength reduction factors for the considered notched specimens (fatigue strength reduction factors are determined/estimated at $N_A = 2 \bullet 10^6$ cycles to failure).

Material	Ref.	d_n [mm]	d_g [mm]	r_n [mm]	α [°]	K_t	K_{tt}	$K_{f,est}$	$K_{f,exp}$	$K_{ft,est}$	$K_{ft,exp}$	Estimation Formula
C40 Steel (1)	[65]	12	20	0.5	90	3.68	1.95	2.99	2.24	1.79	1.28	Eqs (5) to (8)
En3B	[10]	5	8	0.2	60	3.80	2.10	2.43	3.93	1.70	1.67	Eqs (5) to (8)
		5	8	1.25	60	1.80	1.30	1.69	–	1.27	–	
		5	8	4	–	1.30	1.10	1.29	–	1.10	–	
SAE 1045	[66]	40	50	5	–	1.42	1.23	1.40	1.04	1.22	–	Eqs (5) to (8)
Low Carbon Steel	[67]	7.62	12.7	0.2	35	4.60	2.40	2.36	3.23	1.70	1.52	Eqs (5) to (8)
		7.62	12.7	0.4	35	3.40	1.90	2.31	2.27	1.60	1.20	
39NiCrMo3	[68]	12	20	0.1	90	7.46	3.17	4.30	2.00	2.38	–	Eqs (5) to (8)
AISI 416	[11]	12	20	0.1	90	7.46	3.17	3.31	3.59	2.04	1.03	Eqs (5) to (8)
		16	20	0.1	90	7.62	3.36	3.36	3.68	2.13	1.02	
		19	20	0.1	90	5.35	2.83	2.55	1.92	1.88	1.12	
EN-GJS400	[69,70]	12	20	0.1	90	7.46	3.17	2.12	1.69	1.06	–	Eqs (9) and (10)
2024-T3	[71,72]	25.4	29	1.6	–	3.22	3.83	2.59	1.74	3.03	2.35	Eqs (5) and (6) with $a_P = a_{Pt} = 0.635$ [30]
Al 7050-T7451	[73]	10	15	0.1	60	7.29	3.29	1.86	2.00	1.31	–	Eqs (5) and (6) with $a_P = a_{Pt} = 0.635$ [30]
C40 Steel (2)	[14]	9.15	12	0.225	35	4.42	2.38	3.19	3.28	2.03	–	Eqs (5) to (8)
		9	12	1.2	90	2.19	1.42	2.08	–	1.40	–	
		9	12	3	–	1.62	1.21	1.59	–	1.20	–	
En8	[17]	18	38	1.5	0	2.69	1.34	2.51	2.95	1.32	–	Eqs (5) to (8)
		18	38	3	0	2.12	1.24	2.06	–	1.23	–	
		18	38	6	–	1.72	1.20	1.70	–	1.20	–	
AISI 316 L	[74]	8	12	0.07	90	7.17	3.12	1.51	–	1.17	–	Eqs (3) and (4) with q = 0.082
		8	12	2	90	1.77	1.27	1.07	–	1.00	–	
		8	12	5	–	1.35	1.12	1.00	–	1.00	–	

(either in-phase or 90° out-of-phase) biaxial loading the ratio between the amplitude of the axial nominal stress and the amplitude of the nominal torsional stress was kept constant and equal to unity. The load ratio was set equal to −1 and to 0.

The notched specimens of En3B [10] were tested under in-phase and 90° out-of-phase tension and torsion, with the load ratio being set equal to −1 as well as to 0. Two different ratios between the amplitudes of the tensile and torsional net stress were investigated, i.e., 1 and $\sqrt{3}$. The fatigue tests were run at a frequency ranging between 6 and 10 Hz.

The specimens of normalised SAE 1045 [66] were manufactured from 63.5 mm diameter hot rolled bars. After being polished to a mirror finish, the SAE shafts with fillet were tested under cyclic bending and torsion applied using hydraulic load-controlled test rigs. Fatigue lifetime was defined as the number of cycles to failure needed to initiate and growth a superficial crack having length equal to 1 mm.

The notched specimens of low carbon steel [67] were tested under in-phase fully-reversed loading, with the ratio between the amplitudes of the tensile and torsional net stress being set equal to 2.

The notched samples tested by Berto et al. [68] were made of hardened and tempered steel 39NiCrMo3 with a very fine and isotropic microstructure. The tests were run at a frequency ranging from 1 Hz up to 10 Hz. Under in-phase and 90° out-of-phase biaxial loading the ratio between the amplitudes of the axial and the torsional nominal stresses was set equal to 0.6, 1 and 1.6, with the load ratio being equal to either −1 or to 0.

The notched specimens made of hardened and tempered steel AISI 416 tested by Berto and Lazzarin [11] were characterised by a martensitic microstructure. Before testing, all the specimens were polished to achieve a mirror finish. Axial, torsional, and in-phase/90° out-of-phase biaxial tests were run at a frequency ranging in the interval 5–15 Hz. The load ratio was set equal either to −1 or to 0. The ratio between the amplitudes of the axial and the torsional nominal stresses was set equal to 0.6 and 1.2.

The specimens used by Berto, Lazzarin, Tovo and Cova [69,70] were made of ductile cast iron EN-GJS400 having nodule count equal to 50 nod. No/mm^2 (x100), nodularity equal to 80–85%, average nodule size equal to 50 μm and percentage of ferrite equal to 90%. As reported in Ref. [70], the material used to manufacture the specimens was taken from the critical region of a real component. The tests were run at the frequency varying in the range 1–15 Hz, with the load ratio, R, being set either equal to 0 or to −1. The results under in-phase and 90° out-of-phase biaxial loading were generated by setting the ratio between the amplitudes of the torsional and the axial nominal stresses equal to 0.6 and 1.

The holed tubular specimens tested by Gates and Fatemi [71,72] were made of commercial aluminium alloy 2024-T3. The specimens were machined from the parent drawn tubes having nominal outer diameter equal to 34.9 mm and nominal inner diameter equal to 25.4 mm. Both the internal and the external surfaces of the samples were polished and the 3.2 mm diameter hole was manufactured via conventional drilling and reaming. Finally, the specimens were lightly polished again to remove the drilling burrs. The biaxial tests were carried out under in-phase and 90° out-of-phase fully-reversed tension and torsion, with the frequency ranging from 0.2 Hz up to 7 Hz.

Both the plain and notched specimens of Al 7050-T7451 [73] were machined so that their longitudinal axes were parallel to the longitudinal direction of the parent material block. Detailed microstructural analyses revealed that the tested specimens contained equiaxed grains. The experimental tests were run under force/torque controlled fully-reversed sinusoidal loading, with the adopted failure criterion being the complete separation of the specimens. The biaxial fatigue results were generated under in-phase combined tension and torsion by setting the ratio between the amplitudes of the axial and the torsional nominal stresses equal to $5\sqrt{3/4}$ and $2\sqrt{3}$.

The plain and notched specimens of both C40 [14] and unalloyed medium carbon steel En8 (080 M40) [17] were manufactured using a conventional lathe, with notches of different sharpness being obtained by changing the root radius of the tool bits. As far as specimens of C40 [14] are concerned, uniaxial, torsional and biaxial tests were run, at maximum frequency of 4 Hz, by adopting a triangular shape for the wave form. Fatigue failures were defined by using the 50% stiffness drop criterion. In contrast, the specimens of En8 [17] were tested under CA/VA sinusoidal loading signals, with the frequency varying in the range 0.5 to 2 Hz. For these tests the number of cycles/blocks to failure was defined by 5% axial/torsional stiffness drop. The biaxial fatigue results from the specimens of both C40 [14] and En8 (080 M40) [17] were generated considering in-phase as well as 90° out-of-phase biaxial load histories, the load ratios being set not only equal to −1, but also equal to

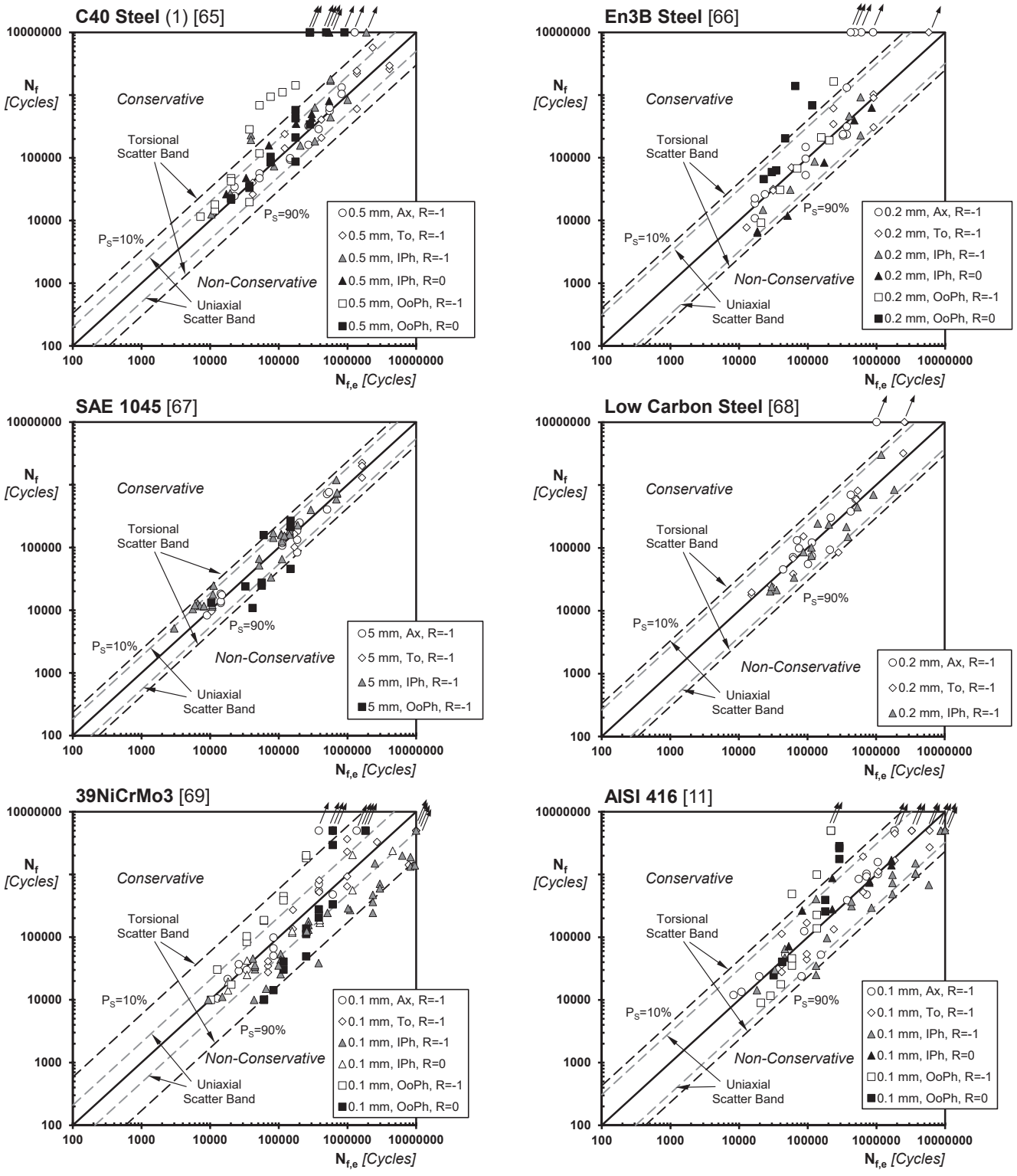

Fig. 6. Accuracy of the MWCM in estimating CA multiaxial notch fatigue strength when the criterion is calibrated using experimentally generated fatigue curves – the experimental results in the graphs are classified according to the notch root radius, r_n, and the type of loading (Ax = Axial loading; To = Torsion; IPh = In-phase loading; OoPh = 90° Out-of-phase loading).

0.

The 3D-printed samples of 316L stainless steel tested by Wang et al. [74] were additively manufactured using the Selective Laser Melting (SLM) technology, where the laser power was set equal to 450 W, the scan speed to 1500–2000 mm/s, and the scan pitch to 0.05 mm. Both the plain and the notched specimens were fabricated using a conventional lathe from rods that were 3D-printed flat on the build plate. Before the final manufacturing, the parent rods were annealed for 6 h at a temperature of 490 °C and then cooled down in argon. The fatigue tests were run under force/torque control at a frequency ranging between 1 Hz and

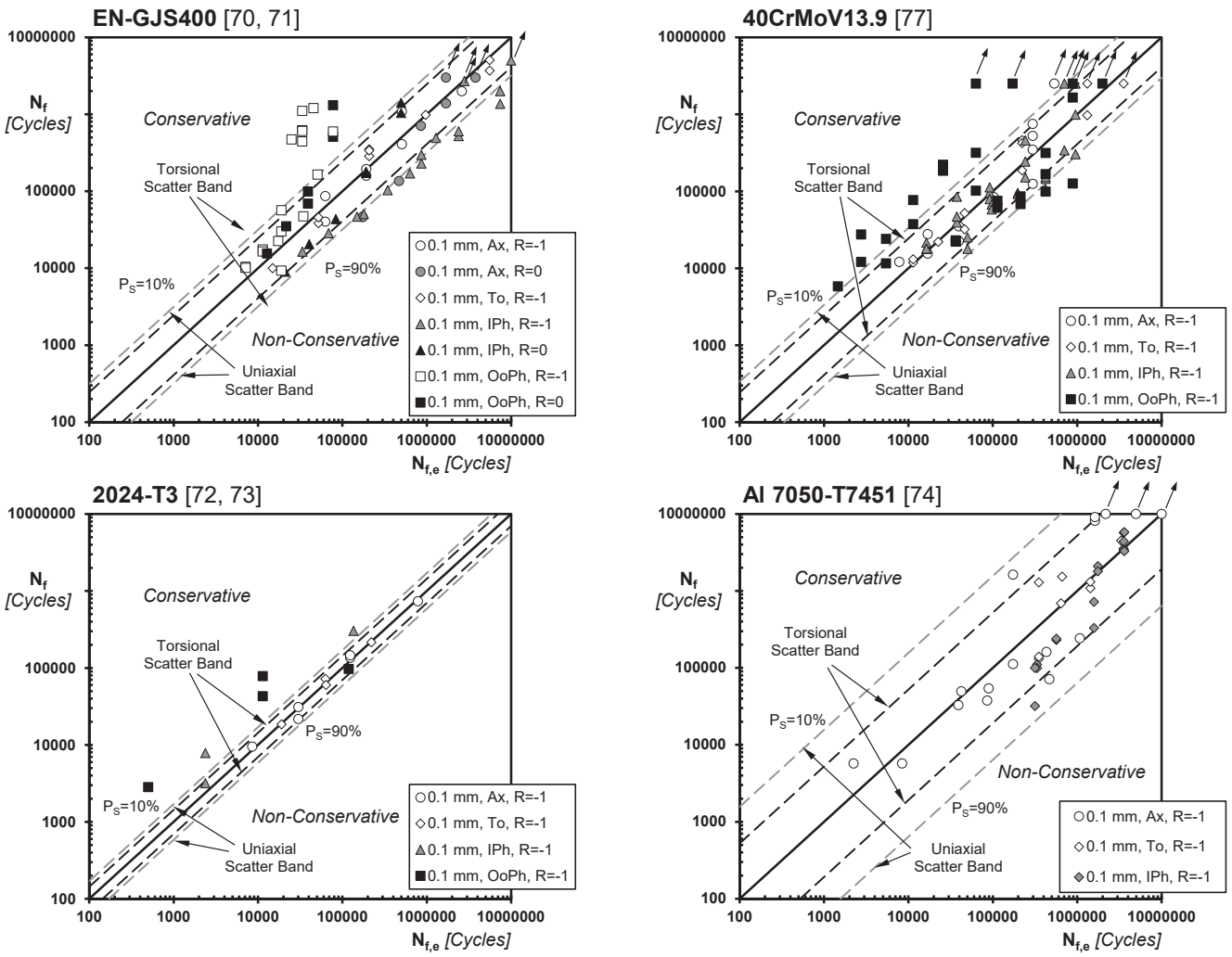

Fig. 6. (*continued*).

8 Hz. These results were generated by exploring load ratios equal to both −1 and 0, with the biaxial tests being run under both in-phase and 90° out-of-phase tension and torsion. Independently of the complexity of the load history being investigated, the experimental number of cycles to failure was defined as the number of cycles needed to initiate and grow cracks having length equal to about 1 mm.

The notched specimens tested by Berto, Lazzarin and Marangon [75] were made of steel 40CrMoV13.9 having a high strength bainitic/martensitic structure. The steel bars used to make these samples were quenched at 920 °C, tempered twice at about 580 °C and, finally, stress relieved at 570 °C. Axial, torsional, and in-phase/90° out-of-phase biaxial tests were run, under a load ratio equal to −1, at a frequency ranging from 1 Hz up to 10 Hz. The ratio between the amplitudes of the torsional and the axial nominal stresses was set equal to 0.6 and 1.1.

The values of the axial, K_t, and torsional, K_{tt}, stress concentration factors characterising the notched samples being re-analysed are summarised in Table 3. These values were taken from the original sources and, when possible, double-checked using Peterson's book [76].

In order to assess the actual accuracy of the MWCM, initially we extracted from our data base those data sets for which the calibration fatigue curves could be determined rigorously by post-processing experimental results generated under both axial and torsional fully-reversed loading. The calibration fatigue curves for these initial validation data sets are summarised in Table 1. For the various materials/notch geometries listed in this table the calibration fatigue curves are reported in terms of nominal net endurance limit, σ_{An} and τ_{An}, extrapolated at $N_A = 2 \bullet 10^6$ cycles to failure and negative inverse slope, k and k_0. These fatigue curves were determined by assuming a log-normal distribution of the cycles to failure for any stress level, with the confidence being set equal to 95% [77,78]. The level of scattering characterising the calibration fatigue curves calculated according to this procedure was quantified in terms of ratio between the endurance limits determined for 10% and 90% probability of survival - T_σ for the uniaxial case and T_τ for the torsional case. This rigorous statistical procedure was used not only to determine the notch calibration fatigue curves listed in Table 1, but also the plain fatigue curve reported in Table 2.

For those materials listed in Table 1 for which the plain uniaxial and torsional fully-reversed curves could be determined by post-processing suitable results, the experimental values of the fatigue strength reduction factors under axial loading, $K_{f,exp}$, as well as under torsional loading, $K_{ft,exp}$, are reported in Table 3.

The mean stress sensitivity index, m, was taken invariably equal to 0.2 for steel En3B [10]. As far as the notched specimens of SAE 1045 [66] are concerned, ρ_{lim} was calculated to be equal to 1.26 and to 1.9 when the MWCM was calibrated via experimental and estimated fatigue curves, respectively. As suggested in Ref. [74], the experimental results generated by testing notched 3D-printed specimens of AISI 316 L were post-processed by taking $\rho_{lim} = 1.45$ and $m = 0.53$. For the other materials m and ρ_{lim} were taken invariably equal to unity.

The estimated, $N_{f,e}$, vs. experimental, N_f, number of cycles to failure diagrams seen in Fig. 6 summarise the overall accuracy of the MWCM when this criterion is calibrated through experimentally determined

Table 4
Summary of the calibration fatigue curves estimated under axial as well as under torsional fatigue loadin.

Material	Ref.	d_n	d_g	r_n	α	Uniaxial Loading			Torsional Loading			$K_{f,est}$	$K_{ft,est}$
						R	σ_{An} [(1)]	k	R	τ_{An} [(1)]	k_0		
		[mm]	[mm]	[mm]	[°]		[MPa]			[MPa]			
C40 Steel (1)	[65]	12	20	0.5	90	−1	88.4	4.94	−1	109.6	7.62	2.99	1.79
En3B	[10]	5	8	0.2	60	−1	137.4	5.97	−1	152.1	8.11	2.43	1.70
		5	8	1.25	60	−1	197.6	8.35	−1	203.5	11.78	1.69	1.27
		5	8	4	–	−1	258.8	11.87	−1	235.0	15.15	1.29	1.10
SAE 1045	[66]	40	50	5	–	−1	139.9	6.45	−1	94.9	8.04	1.40	1.22
Low Carbon Steel	[67]	7.62	12.7	0.2	35	−1	91.6	5.59	−1	110.1	8.80	2.36	1.70
		7.62	12.7	0.4	35	−1	93.6	5.68	−1	116.9	9.46	2.31	1.60
39NiCrMo3	[68]	12	20	0.1	90	−1	73.3	3.03	−1	111.5	4.56	4.30	2.38
AISI 416 steel	[11]	12	20	0.1	90	−1	105.6	5.23	−1	110.5	6.50	3.31	2.04
		16	20	0.1	90	−1	104.0	5.18	−1	105.8	6.27	3.36	2.13
		19	20	0.1	90	−1	137.1	6.38	−1	119.9	6.99	2.55	1.88
EN-GJS400	[69,70]	12	20	0.1	90	−1	67.1	5.66	−1	129.8	9.35	2.12	1.06
2024-T3	[71,72]	29	29	1.6	–	−1	60.9	3.76	−1	42.7	4.15	2.59	3.03
Al 7050-T7451	[73]	10	15	0.1	60	−1	57.2	3.97	−1	65.4	4.17	1.86	1.31
C40 Steel (2)	[14]	9.15	12	0.225	35	−1	85.3	3.86	−1	108.1	5.84	3.19	2.03
		9	12	1.2	90	−1	130.8	4.93	−1	156.8	8.17	2.08	1.40
		9	12	3	–	−1	171.1	5.97	−1	182.9	9.79	1.59	1.20
En8	[17]	18	38	1.5	0	−1	68.2	4.38	−1	119.6	9.01	2.51	1.32
		18	38	3	0	−1	83.1	4.94	−1	128.4	9.83	2.06	1.23
		18	38	6	–	−1	100.7	5.65	−1	131.6	10.15	1.70	1.20
AISI 316 L	[74]	8	12	0.07	90	−1	164.9	9.10	−1	184.3	20.92	1.51	1.17
		8	12	2	90	−1	233.6	13.84	−1	216.1	32.70	1.07	1.00
		8	12	5	–	−1	249.0	15.30	−1	216.1	32.70	1.00	1.00

(1) Endurance limits extrapolated at $N_A = 2 \bullet 10^6$ cycles to failure.

uniaxial and torsional fatigue curves. The results reported in Fig. 6 were all generated under CA fatigue loading. The error bands plotted in these charts were determined for a probability of survival, P_S, equal to 10% and 90%. They were calculated by directly post-processing the calibration results generated under axial and torsional fully-reversed fatigue loading. The $N_{f,e}$ vs. N_f charts of Fig. 6 demonstrate that the MWCM is highly accurate when the constants in its governing equations are determined through appropriate experiments. In particular, its usage is seen to result in estimates mainly falling within the larger scatter band between the two used to calibrate the method itself. Certainly, this level of accuracy is satisfactory, since, from a statistical viewpoint, it is unrealistic to expect a predictive method to be less scattered than the experimental information used to calibrate the method itself.

The subsequent step in the validation exercise being performed was to assess the MWCM's reliability when the necessary calibration fatigue curves are estimated according to the classic empirical strategies summarised in Section 2. To this end, when they were available in the original sources, the plain material experimental results generated under axial and torsional fully-reversed loading were post-processed in order to obtain the corresponding fatigue curves. The results from the statistical re-analyses are summarised in Table 2.

The fatigue strength reduction factors through which the calibration notch fatigue curves were derived are listed in Table 3 for the axial, $K_{f,est}$, and torsional, $K_{ft,est}$, cases. The empirical equations/values used to estimate these factors are indicated in the same table.

As to the $K_{f,est}$ and $K_{ft,est}$ values reported in Table 3 for additively manufactured AISI 316L, it is important to point out that the strategy being adopted was different from the one followed for the other conventional metallic materials. In particular, due to the differences at a microstructural level deriving from the 3D-printing technology, it is well-known that the classical formulas suitable for estimating the fatigue strength reduction factors do not always return reliable values [60]. Accordingly, for this material $K_{f,est}$ and $K_{ft,est}$ were estimated directly from Eqs (3) and (4) by setting q equal to 0.082. This value for the notch sensitivity factor was derived from the $K_{f,exp}$ value determined from the plain endurance limit and the endurance limit determined by testing V-notched cylindrical specimens with notch root radius, r_n, equal to 0.07 mm.

Having estimated the values of the required fatigue strength reduction factors, the calibration notch fatigue curves summarised in Table 4 were directly derived from the plain fatigue curves listed in Table 2. According to Fig. 1b, N_S in the low cycle fatigue regime was set equal to 10^3 cycles to failure [42] for all the conventional metallic material being considered. In contrast, for 3D printed AISI 316 L N_S was calculated to be equal 191 cycles to failure, with this value being obtained from the intersecting point between the plain fatigue curve and the fatigue curve generated by testing the notched specimens with $r_n = 0.07$ mm.

The $N_{f,e}$ vs N_f error charts reported in Fig. 7 summarise the accuracy of the MWCM in estimating CA fatigue lifetime when the approach is calibrated using the estimated uniaxial and torsional fatigue curves reported in Table 4. These diagrams make it evident that the MWCM is still capable of estimates falling mainly within an error factor of 3, with just a few estimates being on the non-conservative side. Given the accuracy characterising the predictions summarised in Fig. 6, clearly the increased level of scattering associated with the estimates shown in Fig. 7 is to be ascribed to the approximations that are inevitably introduced when the calibration information is guessed via the empirical equations/values reviewed in Section 2. In this context, it can be pointed out that, while it is relatively high, the level of scattering characterising the predictions made for additively manufactured AISI 316 L is comparable with the experimental one characterising the $r_n = 0.07$ mm notch fatigue curve used to estimate the material notch sensitivity, q (Table 3).

Having checked the accuracy of the MWCM applied in terms of nominal stresses in the presence of CA fatigue loading, the subsequent step in the validation process was to consider experimental results generated under VA multiaxial load histories. Fig. 8 summarises the load spectra that were considered in the present investigation.

The cylindrical specimens with a through-thickness hole of 2024-T3 [16,71,72] were tested considering two stress-based loading histories simulating a number of events damaging the lower wing skin of a military aircraft. The axial and torsional channels of the complete load histories contained 436,098 and 422,071 cycles, respectively (Fig. 8). The edited versions of this load history were built in order to reduce the length of the two stress channels, with this being done to retain about 90% of the total initial damage. The simplified load histories resulted in

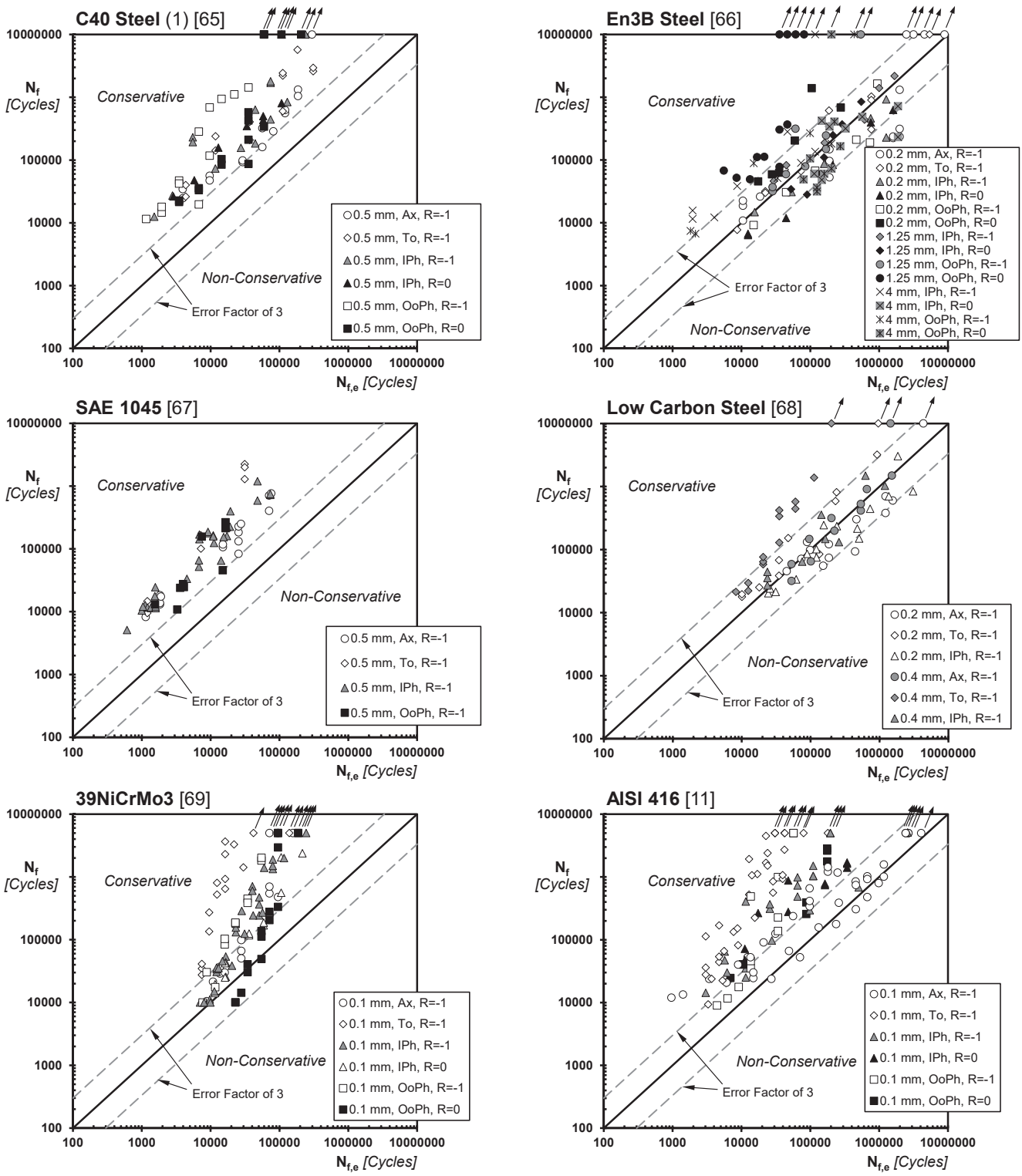

Fig. 7. Accuracy of the MWCM in estimating CA multiaxial notch fatigue strength when the method is calibrated via calibration fatigue curves that are estimated – the experimental results in the graphs are classified according to the notch root radius, r_n, and the type of loading (Ax = Axial loading; To = Torsion; IPh = In-phase loading; OoPh = 90° Out-of-phase loading).

about $3 \bullet 10^4$ cycles under axial loading and about $2 \bullet 10^4$ cycles under torsion (Fig. 8). The first two charts in Fig. 9 show the accuracy of the MWCM applied in conjunction with the nominal stress approach in estimating the VA fatigue lifetime of the notched specimens of 2024-T3 [16]. These error diagrams summarise the accuracy of our approach when it was calibrated using the experimental (Table 1) and estimated (Table 4) fatigue curves, respectively. The estimates reported in these two charts were obtained by adopting the 2 k-1 correction – Eq. (27), with the knee point being taken at $2 \bullet 10^6$ cycles to failure. These two error diagrams make it evident that the MWCM was successful in

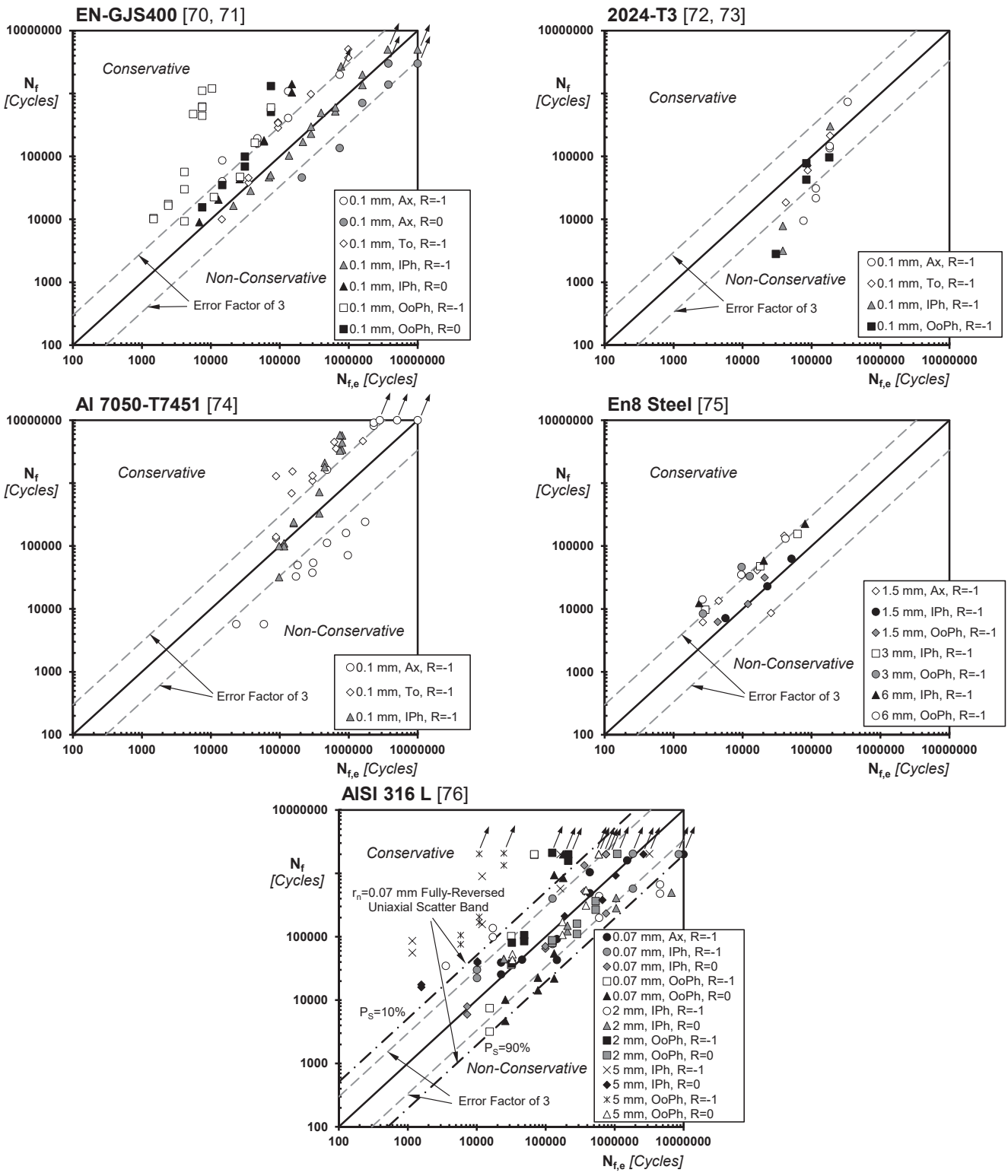

Fig. 7. (*continued*).

estimating the VA fatigue lifetime of the notched aluminium specimens tested by Gates and Fatemi [16]. As far as these predictions are concerned, it is important to highlight that such a high level of accuracy was achieved by setting the critical value of the damage sum, D_{cr}, equal to 0.05. This fact is not at all surprising since, as pointed out by Sonsino [58], for aluminium alloys D_{cr} is seen to vary in the range 0.02-5, with the average value being equal to 0.37.

The notched specimens of C40 steel [14], En8 [17] and AISI 316 L [74] were tested under VA fatigue loading by using the concave upwards spectra seen in Fig. 8. These experimental investigations were run to explore the effect of in-phase and 90° out-of-phase VA loading as well as of non-zero mean stresses. Further, the notched specimens of C40 steel [14] and En8 [17] were tested by changing also the ratio, F, between the frequencies of the axial and torsional loading channels.

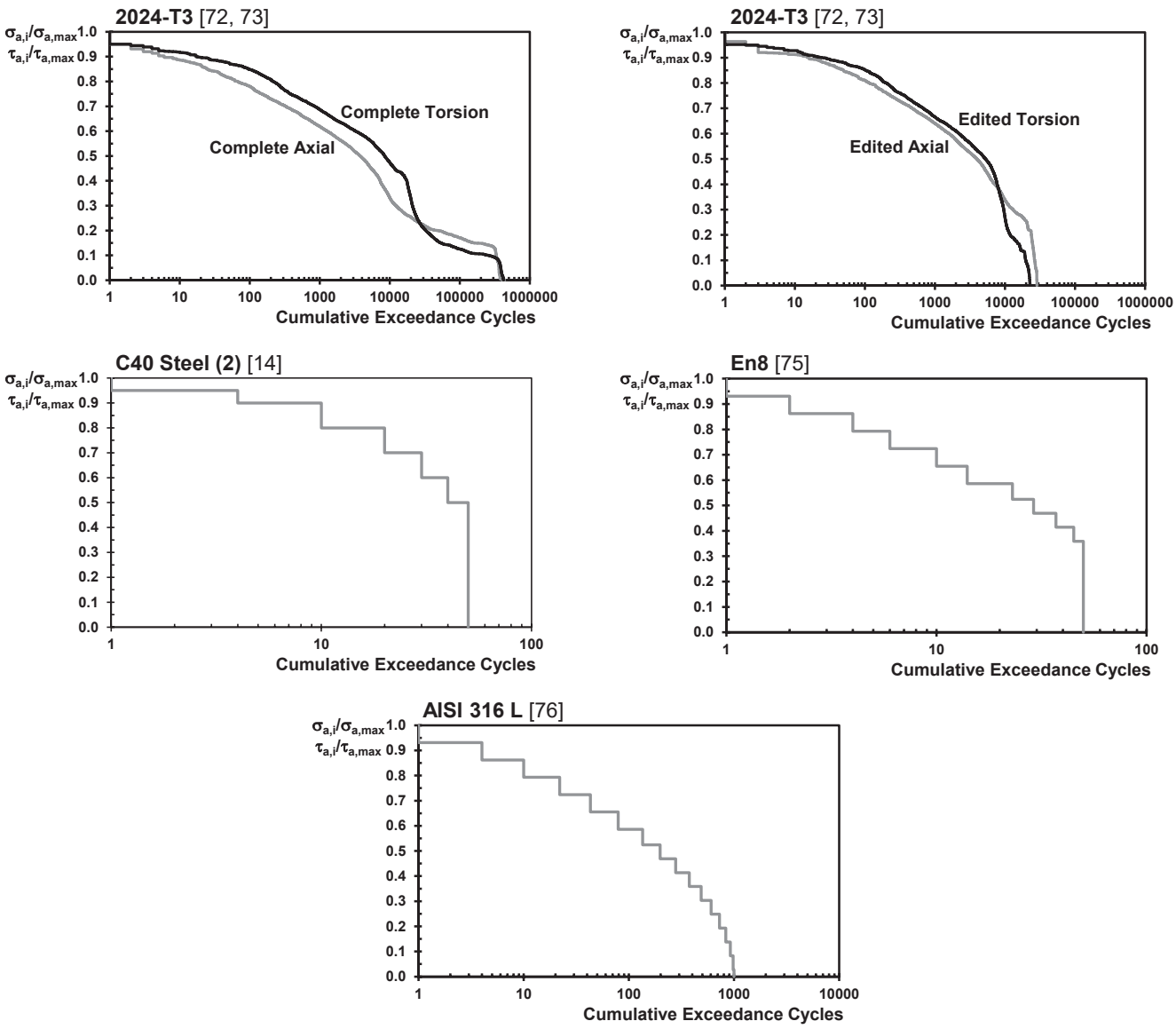

Fig. 8. Investigated load spectra.

The predictions summarised in the error diagrams of Fig. 9 were made by calibrating the MWCM via the estimated uniaxial and torsional fatigue curves reported in Table 4. Further, the VA fatigue lifetime of these notched specimens was predicted by adopting the 2k-1 correction – Eq. (20), with the knee point being taken at $2 \bullet 10^6$ cycles to failure. The critical value of the damage sum was set equal to unity.

The error diagrams summarising the estimates obtained for the notched specimens of C40 [14], En8 [17] and AISI 316 L [74] make it evident that the MWCM applied in terms of nominal stresses was highly accurate and reliable also when it was used to predict these VA experimental results. This level of accuracy is certainly satisfactory, especially in light of the fact that these predictions were made by calibrating the MWCM via uniaxial and torsional fatigue curve that were estimated as summarised in Table 4.

6. Conclusions

In the present investigation, the accuracy and reliability in estimating notch fatigue strength of the MWCM applied in terms of nominal stresses assessed systematically against a large number of experimental results. The considered literature data sets were generated under both constant and variable amplitude uniaxial/multiaxial load histories, with these experimental campaigns being run to investigate the effect of non-proportional loading as well as of superimposed static stresses. This systematic validation exercise was implemented by calibrating the MWCM not only experimentally, but also through uniaxial and torsional fatigue curves that were estimated using a number of classic empirical formulas.

Based on the re-analyses that were discussed in the present paper, as long as the MWCM is used in conjunction with the nominal stress approach to estimate notch fatigue strength, the most relevant conclusions are summarised in the following bullet points.

- When calibrated experimentally for a probability of survival equal to 50%, the MWCM is seen to return estimates mainly falling within the larger scatter band between the two associated with the uniaxial and torsional calibration fatigue curves.
- The MWCM can be calibrated by estimating the necessary uniaxial and torsional fully-reversed design curves. However, under these circumstances, this method is recommended to be used not only by considering calibration curves characterised by an adequate value of

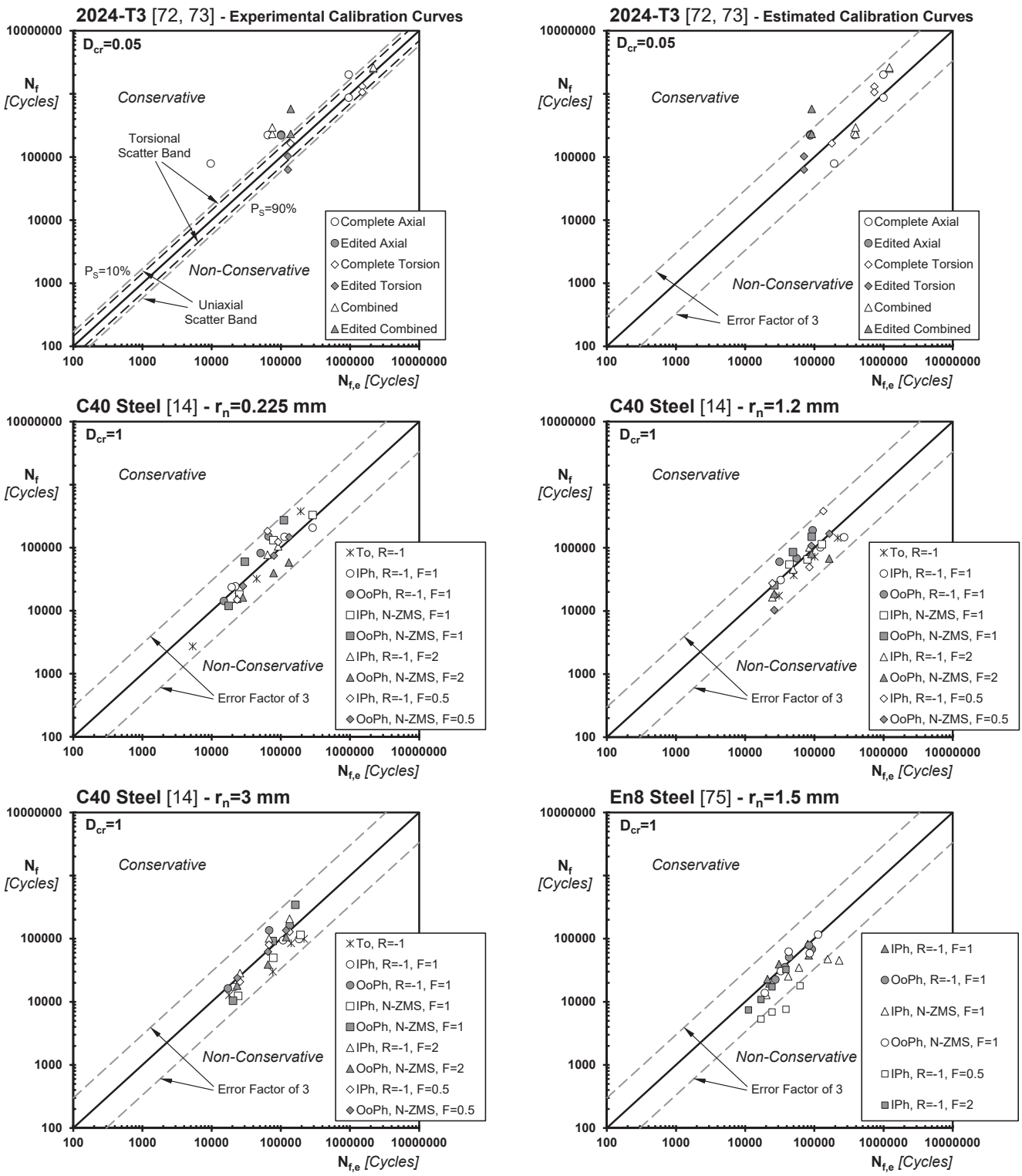

Fig. 9. Accuracy of the MWCM applied in terms of nominal stresses in estimating VA multiaxial notch fatigue strength – the experimental results in the graphs are classified according to the notch root radius, r_n, and the type of loading (To = Torsion; IPh = In-phase loading; OoPh = 90° Out-of-phase loading; N-ZMS = Non-zero mean stress).

the probability of survival, but also by adopting suitable safety factors.

- When calibrated through fatigue curves estimated for a probability of survival equal to 50%, the MWCM is seen to be capable of predictions failing mainly (on the conservative side) within an error factor of 3.
- Independently of the strategy used for its calibration, the MWCM is proven to be highly accurate in estimating notch fatigue lifetime under VA multiaxial load histories.

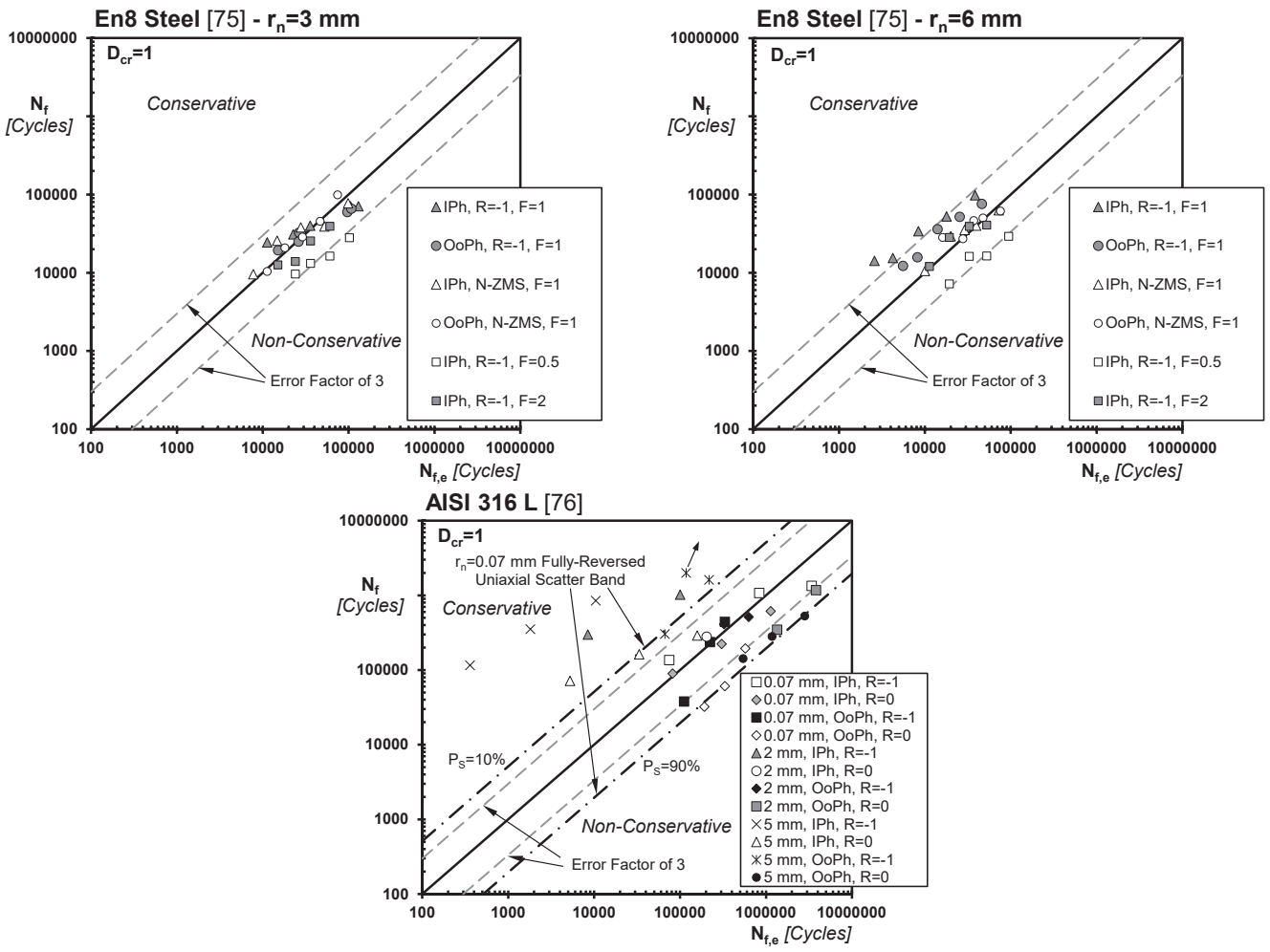

Fig. 9. (*continued*).

- When the MWCM is used to design notched components against VA loading, care must be taken to set the critical value of the damage sum reliably.

Declaration of Competing Interest

The authors declare that they have no known competing financial interests or personal relationships that could have appeared to influence the work reported in this paper.

References

[1] McKelvey S, Zhang S, Subramanian E, Lee Y-L. Review and Assessment of Multiaxial Fatigue Limit Models. SAE Technical Paper 2020-01-0192, 2020, doi: 10.4271/2020-01-0192.
[2] Bagni C, Askes H, Susmel L. Gradient elasticity: a transformative stress analysis tool to design notched components against uniaxial/multiaxial high-cycle fatigue. Fatigue Fract Eng Mater Struct 2016;39(8):1012–29.
[3] Sonsino CM. Multiaxial fatigue life response depending on proportionality grade between normal and shear strains/stresses and material ductility. Int J Fatigue 2020;135:105468. https://doi.org/10.1016/j.ijfatigue.2019.105468.
[4] Leitner M, Vormwald M, Remes H. Statistical size effect on multiaxial fatigue strength of notched steel components. Int J Fatigue 2017;104:322–33.
[5] Riess C, Hiese W, Obermayr M, Vormwald M. Engineering approaches to multiaxial and non-proportional fatigue of notched components. Mat-wiss u Werkstofftech 2018;49(3):381–91.
[6] Liu J, Ran Y, Xie L, Xue W. Multiaxial fatigue life prediction method of notched specimens considering stress gradient effect. Fatigue Fract Eng Mater Struct 2021; 44(5):1406–19.
[7] Branco R, Costa JD, Borrego LP, Berto F, Razavi SMJ, Macek W. Comparison of different one-parameter damage laws and local stress-strain approaches in multiaxial fatigue life assessment of notched components. Int J Fatigue 2021;151: 106405. https://doi.org/10.1016/j.ijfatigue.2021.106405.
[8] Susmel L, Taylor D. Two methods for predicting the multiaxial fatigue limits of sharp notches. Fatigue Fract Eng Mater Struct 2003;26(9):821–33.
[9] Susmel L. A unifying approach to estimate the high-cycle fatigue strength of notched components subjected to both uniaxial and multiaxial cyclic loadings. Fatigue Fract Eng Mater Struct 2004;27(5):391–411.
[10] Susmel L, Taylor D. The modified Wöhler curve method applied along with the theory of critical distances to estimate finite life of notched components subjected to complex multiaxial loading paths. Fatigue Fract Eng Mater Struct 2008;31(12): 1047–64.
[11] Berto F, Lazzarin P. Fatigue strength of structural components under multi-axial loading in terms of local energy density averaged on a control volume. Int J Fatigue 2011;33(8):1055–65.
[12] Gates N, Fatemi A. Notched fatigue behavior and stress analysis under multiaxial states of stress. Int J Fatigue 2014;67:2–14.
[13] Liao D, Zhu S-P, Qian G. Multiaxial fatigue analysis of notched components using combined critical plane and critical distance approach. Int J Mech Sci 2019;160: 38–50.
[14] Susmel L, Taylor D. A critical distance/plane method to estimate finite life of notched components under variable amplitude uniaxial/multiaxial fatigue loading. Int J Fatigue 2012;38:7–24.
[15] Gates N, Fatemi A. Multiaxial variable amplitude fatigue life analysis including notch effects. Int J Fatigue 2016;91:337–51.
[16] Gates NR, Fatemi A. Multiaxial variable amplitude fatigue life analysis using the critical plane approach, Part II: Notched specimen experiments and life estimations. Int J Fatigue 2018;106:56–69.
[17] Faruq NZ, Susmel L. Proportional/non-proportional constant/variable amplitude multiaxial notch fatigue: cyclic plasticity, non-zero mean stresses, and critical distance/plane. Fatigue Fract Eng Mater Struct 2019;42(9):1849–73.
[18] Rennert R, Kullig E, Vormwald M, Esderts A, Siegele D. Analytical strength assessment of components made of steel, cast iron and aluminium materials in mechanical engineering, 6th Edition, VDMA Verlag, Frankfurt, Germany, 2012.
[19] Anon. BS 7608, Guide to fatigue design and assessment of steel products, 2014.
[20] Hobbacher AF. Recommendations for Fatigue Design of Welded Joints and Components. Springer International Publishing, 2016, ISBN: 978-3-319-23757-2.

[21] Anon.. DNVGL-RP-C203 - Fatigue design of offshore structures. DNVGL 2019.
[22] Louks R, Gerin B, Draper J, Askes H, Susmel L. On the multiaxial fatigue assessment of complex three-dimensional stress concentrators. Int J Fatigue 2014;63:12–24.
[23] Neuber H. Zur Theorie der technischen Formzahl. Forsch Ing Wes 1936;7(6):271–4.
[24] Peterson RE. Notch sensitivity. In Metal Fatigue, Eds: G. Sines and J. L. Waisman, McGraw-Hill, New York, 1959, pp. 293-306.
[25] Susmel L. Multiaxial Notch Fatigue: from nominal to local stress-strain quantities. Woodhead & CRC, Cambridge, UK, ISBN: 1 84569 582 8, 2009.
[26] Gough HJ. Engineering Steels under Combined Cyclic and Static stresses. Proc Inst Mech Eng 1949;160(1):417–40.
[27] Anon. ENV 1993-1-1, EUROCODE 3, Design of steel structures, 2005.
[28] Anon. EN 1999-1-1, EUROCODE 9, Design of aluminium structures, 2007.
[29] Anon. EN 13000:2010+A1:2014, Cranes - Mobile cranes, 2014.
[30] Susmel L, Lazzarin P. A bi-parametric modified Wöhler curve for high cycle multiaxial fatigue assessment. Fatigue Fract Eng Mater Struct 2002;25:63–78.
[31] Lazzarin P, Susmel L. A stress-based method to predict lifetime under multiaxial fatigue loadings. Fatigue Fract Eng Mater Struct 2003;26(12):1171–87.
[32] Lee Y-L, Pan J, Hathaway RB, Barkey ME. Fatigue Testing and Analysis. Elsevier Butterworth–Heinemann, 2005.
[33] Miller KJ. The two thresholds of fatigue behaviour. Fatigue Fract Eng Mater Struct 1993;16(9):931–9.
[34] Akiniwa Y, Tanaka K, Kimura H. Microstructural effects on crack closure and propagation thresholds of small fatigue cracks. Fatigue Fract Eng Mater Struct 2001;24(12):817–29.
[35] Miller KJ, O'Donnell WJ. The fatigue limit and its elimination. Fatigue Fract Eng Mater Struct 1999;22:545–57.
[36] Sonsino C. Course of SN-curves especially in the high-cycle fatigue regime with regard to component design and safety. Int J Fatigue 2007;29(12):2246–58.
[37] Yao W, Xia K, Gu Y. On the fatigue notch factor, K_f. Int J Fatigue 1995;17:245–51.
[38] Ciavarella M, Meneghetti G. On fatigue limit in the presence of notches: classical vs. recent unified formulations. Int J Fatigue 2004;26:289–98.
[39] Stephens RI, Fatemi A, Stephens RR, Fuchs HO. Metal Fatigue in Engineering. 2nd Edition, Wiley, New York, USA, 2000.
[40] Heywood RE. Designing against fatigue. Chapman and Hall, London, UK; 1962.
[41] Dowling NE. Mechanical Behaviour of Materials. 2nd ed. Prentice-Hall Inc., New Jersey, USA; 1998.
[42] Atzori B. Appunti di Costruzione di Macchine. Ed. Cortina, Padova, Italy (In Italian), 2000.
[43] Susmel L, Tovo R. On the use of nominal stresses to predict the fatigue strength of welded joints under biaxial cyclic loadings. Fatigue Fract Eng Mater Struct 2004;27:1005–24.
[44] Susmel L. Multiaxial fatigue limits and material sensitivity to non-zero mean stresses normal to the critical planes. Fatigue Fract Eng Mater Struct 2008;31(3-4):295–309.
[45] Susmel L, Tovo R, Lazzarin P. The mean stress effect on the high-cycle fatigue strength from a multiaxial fatigue point of view. Int J Fatigue 2005;27(8):928–43.
[46] Karadag M, Stephens RI. The influence of high R ratio on unnotched fatigue behaviour of 1045 steel with three different heat treatments. Int J Fatigue 2003;25:191–200.
[47] Socie D, Bannantine J. Bulk deformation fatigue damage models. Mater Sci Eng A 1988;103(1):3–13.
[48] Kaufman RP, Topper T. The influence of static mean stresses applied normal to the maximum shear planes in multiaxial fatigue. In: Biaxial and Multiaxial fatigue and Fracture, Edited by A. Carpinteri, M. de Freitas and A. Spagnoli, Elsevier and ESIS, 123-143, 2003.
[49] Susmel L, Tovo R, Benasciutti D. A novel engineering method based on the critical plane concept to estimate the lifetime of weldments subjected to variable amplitude multiaxial fatigue loading. Fatigue Fract Eng Mater Struct 2009;32(5):441–59.
[50] Susmel L. A simple and efficient numerical algorithm to determine the orientation of the critical plane in multiaxial fatigue problems. Int J Fatigue 2010;32(11):1875–83.
[51] Susmel L, Tovo R. Estimating fatigue damage under variable amplitude multiaxial fatigue loading. Fatigue Fract Eng Mater Struct 2011;34(12):1053–77.
[52] Susmel L, Tovo R, Socie DF. Estimating the orientation of Stage I crack paths through the direction of maximum variance of the resolved shear stress. Int J Fatigue 2014;58:94–101.
[53] Fatemi A, Socie DF. A critical plane approach to multiaxial fatigue damage including out-of-phase loading. Fatigue Fract Eng Mater Struct 1988;11(3):149–65.
[54] Socie DF. Multiaxial fatigue damage models. J Eng Mater Technol 1987;109:293–8.
[55] Wang CH, Brown MW. A path-independent parameter for fatigue under proportional and non-proportional loading. Fatigue Fract Eng Mater Struct 1993;16(12):1285–97.
[56] Susmel L. Four stress analysis strategies to use the Modified Wöhler Curve Method to perform the fatigue assessment of weldments subjected to constant and variable amplitude multiaxial fatigue loading. Int J Fatigue 2014;67:38–54.
[57] Luo P, Yao W, Susmel L. An improved critical plane and cycle counting method to assess damage under variable amplitude multiaxial fatigue loading. Fatigue Fract Eng Mater Struct 2020;43(9):2024–39.
[58] Sonsino C. Fatigue testing under variable amplitude loading. Int J Fatigue 2007;29(6):1080–9.
[59] Haibach E. Betriebsfestigkeit—Verfahren und Daten zur Bauteilberechnung. VDI-Verlag GmbH, Düsseldorf, Germany, 1989.
[60] Matsuishi M, Endo T. Fatigue of metals subjected to varying stress. Presented to the Japan Society of Mechanical Engineers, Fukuoka, Japan, 1968.
[61] Palmgren A. Die Lebensdauer von Kugellagern. Verfahrenstechnik, Berlin 1924;68:339–41.
[62] Miner MA. Cumulative damage in fatigue. J Appl Mech 1945;67:AI59-AI64.
[63] Sonsino CM, Kueppers M. Multiaxial fatigue of welded joints under constant and variable amplitude loadings. Fatigue Fract Eng Mater Struct 2001;24(5):309–27.
[64] Hänel B, Haibach E, Seeger T, Wirthgen G, Zenner H. FKM-Guideline – Analytical Strength Assessment of Components in Mechanical Engineering, 5th Extended Edition, VDMA Verlag, Frankfurt, Germany, 2007.
[65] Atzori B, Berto F, Lazzarin P, Quaresimin M. Multi-axial fatigue behaviour of a severely notched carbon steel. Int J Fatigue 2006;28(5-6):485–93.
[66] Kurath P, Downing SD, Galliart D. R. Summary of non-hardened notched shaft round robin program. In: Multiaxial Fatigue (edited by G. E. Leese and D. F. Socie), AE-14, Society of Automotive Engineers, pp. 13–32, 1989.
[67] Quilafku G, Kadi N, Dobranski J, Azari Z, Gjonaj M, Pluvinage G. Fatigue specimens subjected to combined loading. Role of hydrostatic pressure. Int J Fatigue 2001;23:689–701.
[68] Berto F, Lazzarin P, Yates JR. Multiaxial fatigue of V-notched steel specimens: a non-conventional application of the local energy method. Fatigue Fract Eng Mater Struct 2011;34(11):921–43.
[69] Berto F, Lazzarin P, Tovo R. Multiaxial fatigue strength of severely notched cast iron specimens. Int J Fatigue 2014;67:15–27.
[70] Tovo R, Lazzarin P, Berto F, Cova M, Maggiolini E. Experimental investigation of the multiaxial fatigue strength of ductile cast iron. Theor Appl Fract Mech 2014;73:60–7.
[71] Gates N, Fatemi A. Fatigue crack growth behavior in the presence of notches and multiaxial nominal stress states. Eng Fract Mech 2016;165:24–38.
[72] Gates NR, Fatemi A. On the consideration of normal and shear stress interaction in multiaxial fatigue damage analysis. Int J Fatigue 2017;100:322–36.
[73] Sá MVC, Ferreira JLA, da Silva CRM, Araújo JA. The role of the shear and normal stress gradients on life estimation of notched Al7050-T7451 under multiaxial loadings. Theor Appl Fract Mech 2018;97:38–47.
[74] Wang Y, Wang W, Susmel L. Constant/variable amplitude multiaxial notch fatigue of additively manufactured AISI 316L. Int J Fatigue 2021;152:106412.
[75] Berto F, Lazzarin P, Marangon C. Fatigue strength of notched specimens made of 40CrMoV13.9 under multiaxial loading. Mater Des 2014;54:57–66.
[76] Pilkey WD, Pilkey DF, Bi Z. Peterson's stress concentration factors. 4th Edition, John Wiley & Sons, Inc., 2020.
[77] Anon.. Standard Practice for Statistical Analysis of Linear or Linearized Stress-Life (S-N) and Strain-Life (ε-N) Fatigue Data. ASTM E739 2015.
[78] Al Zamzami I, Susmel L. On the accuracy of nominal, structural, and local stress based approaches in designing aluminium welded joints against fatigue. Int J Fatigue 2017;101(2):137–58.